

Accepted Manuscript

Evaluating the use of amber in palaeoatmospheric reconstructions: The carbon-isotope variability of modern and Cretaceous conifer resins

Jacopo Dal Corso, Alexander R. Schmidt, Leyla J. Seyfullah, Nereo Preto, Eugenio Ragazzi, Hugh C. Jenkyns, Xavier Delclòs, Didier Néraudeau, Guido Roghi

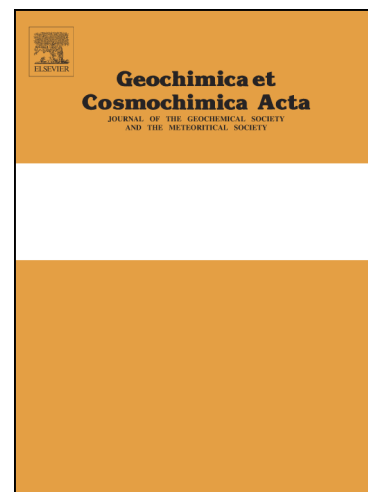
PII: S0016-7037(16)30667-6
DOI: <http://dx.doi.org/10.1016/j.gca.2016.11.025>
Reference: GCA 10033

To appear in: *Geochimica et Cosmochimica Acta*

Received Date: 24 May 2016
Revised Date: 9 November 2016
Accepted Date: 16 November 2016

Please cite this article as: Dal Corso, J., Schmidt, A.R., Seyfullah, L.J., Preto, N., Ragazzi, E., Jenkyns, H.C., Delclòs, X., Néraudeau, D., Roghi, G., Evaluating the use of amber in palaeoatmospheric reconstructions: The carbon-isotope variability of modern and Cretaceous conifer resins, *Geochimica et Cosmochimica Acta* (2016), doi: <http://dx.doi.org/10.1016/j.gca.2016.11.025>

This is a PDF file of an unedited manuscript that has been accepted for publication. As a service to our customers we are providing this early version of the manuscript. The manuscript will undergo copyediting, typesetting, and review of the resulting proof before it is published in its final form. Please note that during the production process errors may be discovered which could affect the content, and all legal disclaimers that apply to the journal pertain.



1 **Evaluating the use of amber in palaeoatmospheric reconstructions: The carbon-isotope**
2 **variability of modern and Cretaceous conifer resins**

3

4 Jacopo Dal Corso^{1,2,3*}, Alexander R. Schmidt⁴, Leyla J. Seyfullah⁴, Nereo Preto¹, Eugenio
5 Ragazzi⁵, Hugh C. Jenkyns⁶, Xavier Delclòs⁷, Didier Néraudeau⁸, Guido Roghi⁹

6

7 ¹Dipartimento di Geoscienze, Università degli Studi di Padova, Via Gradenigo 6, 35131

8 Padova, Italy. *Corresponding author: jacopo.dalcorso@gmail.com

9 ²Dipartimento di Fisica e Scienze della Terra, Università degli Studi di Ferrara, via Saragat 1,
10 44122 Ferrara, Italy.

11 ³Hanse-Wissenschaftskolleg (HWK), Lehmkuhlenbusch 4, 27753 Delmenhorst, Germany.

12 ⁴Abteilung Geobiologie, Georg-August-Universität Göttingen, Goldschmidtstraße 3, 37077
13 Göttingen, Germany.

14 ⁵Dipartimento di Scienze del Farmaco, Università degli Studi di Padova, L.go Meneghetti 2,
15 35131 Padova, Italy.

16 ⁶Department of Earth Sciences, University of Oxford, South Parks Road, Oxford OX1 3AN,
17 UK.

18 ⁷Departament of “Ciències de la Terra i de l’Oceà”, Facultat de Ciències de la Terra,
19 Universitat de Barcelona, Martí i Franques s/n, 08028 Barcelona, Spain.

20 ⁸Université Rennes 1, Géosciences, CNRS UMR 6118, Campus de Beaulieu, Bat. 15, 263
21 Avenue du General Leclerc, Rennes Cedex, France.

22 ⁹Istituto di Geoscienze e Georisorse (IGG-CNR), via Gradenigo 6, 35131 Padova, Italy.

23 **ABSTRACT**

24 Stable carbon-isotope geochemistry of fossilized tree resin (amber) potentially could be a very
25 useful tool to infer the composition of past atmospheres. To test the reliability of amber as a
26 proxy for the atmosphere, we studied the variability of modern resin $\delta^{13}\text{C}$ at both local and
27 global scales. An amber $\delta^{13}\text{C}$ curve was then built for the Cretaceous, a period of abundant
28 resin production, and interpreted in light of data from modern resins. Our data show that
29 hardening changes the pristine $\delta^{13}\text{C}$ value by causing a ^{13}C -depletion in solid resin when
30 compared to fresh liquid-viscous resin, probably due to the loss of ^{13}C -enriched volatiles.
31 Modern resin $\delta^{13}\text{C}$ values vary as a function of physiological and environmental parameters in
32 ways that are similar to those described for leaves and wood. Resin $\delta^{13}\text{C}$ varies between plant
33 species and localities, within the same tree and between different plant tissues by up to 6‰,
34 and in general increases with increasing altitudes of the plant-growing site. We show that, as
35 is the case with modern resin, Cretaceous amber $\delta^{13}\text{C}$ has a high variability, generally higher
36 than that of other fossil tissues. Despite the high natural variability, amber shows a negative
37 2.5–3‰ $\delta^{13}\text{C}$ trend from the middle Early Cretaceous to the Maastrichtian that parallels
38 published terrestrial $\delta^{13}\text{C}$ records. This trend mirrors changes in the atmospheric $\delta^{13}\text{C}$
39 calculated from the $\delta^{13}\text{C}$ and $\delta^{18}\text{O}$ of benthic foraminiferal tests, although the magnitude of
40 the shift is larger in plant material than in the atmosphere. Increasing mean annual
41 precipitation and $p\text{O}_2$ could have enhanced plant carbon-isotope fractionation during the Late
42 Cretaceous, whereas changing $p\text{CO}_2$ levels seem to have had no effect on plant carbon-
43 isotope fractionation. The results of this study suggest that amber is a powerful fossil plant
44 material for palaeoenvironmental and palaeoclimatic reconstructions. Improvement of the
45 resolution of the existing data coupled with more detailed information about botanical source
46 and environmental growing conditions of the fossil plant material will probably allow a more
47 faithful interpretation of amber $\delta^{13}\text{C}$ records and a wider understanding of the composition of
48 the past atmosphere.

49 **Keywords:** Conifer resin, amber, carbon isotopes, palaeoclimate, Cretaceous

50

51 1. INTRODUCTION

52

53 Since C3 plants take up atmospheric CO₂ during photosynthesis and record its carbon-isotope
54 signature, fossil plant remains (such as leaves and wood) can be used to reconstruct the
55 palaeoatmosphere (e.g. Gröcke, 2002; Arens *et al.*, 2000; Bechtel *et al.*, 2008; Diefendorf *et*
56 *al.*, 2010). Plants discriminate against ¹³C during photosynthesis, and the degree of ¹³C
57 fractionation ($\Delta^{13}\text{C}_\text{P}$) depends not only on plant physiology but also on a number of
58 environmental factors and post-photosynthetic $\Delta^{13}\text{C}_\text{P}$ processes, which determine the $\delta^{13}\text{C}$ of
59 plant tissues (Arens *et al.*, 2000; Diefendorf *et al.*, 2010; Schubert and Jahren 2012). The
60 pristine carbon-isotope composition of wood and leaves, the most commonly used tissues in
61 chemostratigraphic analysis, is further changed by diagenesis, through which moieties with
62 different $\delta^{13}\text{C}$ signatures are selectively removed (e.g. van Bergen and Poole, 2002; Bechtel *et*
63 *al.*, 2002). Natural variability and diagenesis make the reconstructions of past atmospheric
64 carbon-isotope composition based on plant $\delta^{13}\text{C}$ analysis difficult because, particularly in
65 deep-time studies, it is often impossible to separate the physiological and environmental
66 effects from atmospheric signals and evaluate the diagenetic effect (Diefendorf *et al.*, 2010).
67 The $\delta^{13}\text{C}$ of fossil wood and leaves ($\delta^{13}\text{C}_\text{WOOD}$ and $\delta^{13}\text{C}_\text{LEAF}$) has been successfully used to
68 infer changes in the carbon-isotope composition of past atmosphere–ocean systems, an
69 approach supported by the evidence of $\delta^{13}\text{C}$ excursions synchronously recorded in both
70 terrestrial organic matter and marine carbonates (e.g. Gröcke, 2002; Strauss and Peters-Kottig,
71 2003; Dal Corso *et al.*, 2011). Records of $\delta^{13}\text{C}_\text{WOOD}$ and $\delta^{13}\text{C}_\text{LEAF}$ parallel those of marine
72 carbonates and can record global long- and short-term perturbations of the carbon cycle, such
73 as the Middle–early Late Triassic 3‰ positive $\delta^{13}\text{C}$ long-term trend (Dal Corso *et al.*, 2011),

74 and the Jurassic and Cretaceous positive and negative shifts associated with oceanic anoxic
75 events (OAEs; e.g. Gröcke, 2002; Hesselbo *et al.*, 2007).

76

77 As a biochemical product of terrestrial plants, amber (fossil tree resin) is expected to record
78 the same $\delta^{13}\text{C}$ shifts recorded by other plant compounds and tissues. Amber is an
79 extraordinary medium for the preservation of animals, plants and fungi that are otherwise rare
80 in the fossil record. It is resistant to diagenesis and can maintain its original chemical and
81 isotopic composition and for this reason is thought to be a very powerful tool for
82 reconstruction of the palaeoatmosphere and the palaeoenvironment (Murray *et al.*, 1998;
83 McKellar *et al.*, 2011; Dal Corso *et al.*, 2011, 2013; Aquilina *et al.*, 2013; Tappert *et al.*,
84 2013). It has been shown that amber $\delta^{13}\text{C}$ ($\delta^{13}\text{C}_{\text{AMBER}}$) falls in the range of typical modern C3
85 plants and may reveal information about climate and environment at the time of resin
86 exudation, for example changes in plant carbon-isotope discrimination linked to
87 environmental stresses such as insect infestation or water availability (Murray *et al.*, 1994,
88 1998; Nissenbaum & Yakir, 1995; McKellar *et al.*, 2008, 2011; Dal Corso *et al.*, 2011, 2013;
89 Tappert *et al.*, 2013). However, contrary to that of wood and leaf, less research has focused on
90 developing amber as a palaeoatmosphere proxy (Tappert *et al.*, 2013). In addition, the lack of
91 sufficient data on the carbon-isotope geochemistry of modern resin, i.e. on the variation of
92 $\delta^{13}\text{C}_{\text{RESIN}}$ (resin $\delta^{13}\text{C}$) under different environmental conditions, renders interpretation of
93 $\delta^{13}\text{C}_{\text{AMBER}}$ problematic.

94

95 Here, as a test case, we explore the value of $\delta^{13}\text{C}_{\text{AMBER}}$ as a proxy for the Cretaceous
96 atmosphere. We studied the variability of modern $\delta^{13}\text{C}_{\text{RESIN}}$ using samples produced by extant
97 conifers from different temperate to tropical environments in order to understand whether
98 resin carbon-isotope behaviour is similar to that of plant tissues. We do not aim to explain the
99 biological and biochemical reasons behind the observed behaviour of modern $\delta^{13}\text{C}_{\text{RESIN}}$ but

100 rather to highlight the patterns and variability that could hamper palaeoclimatic
101 reconstructions and chemostratigraphy. New Cretaceous $\delta^{13}\text{C}_{\text{AMBER}}$ data, coupled with a
102 compilation of published data, were compared in order to combine terrestrial and marine $\delta^{13}\text{C}$
103 records, and interpreted in light of both present-day isotopic variability and the Cretaceous
104 climate.

105

106 2. MATERIAL AND METHODS

107

108 2.1 Methodical background: Factors controlling the $\delta^{13}\text{C}$ of modern C3 plants

109

110 The $\delta^{13}\text{C}$ of C3 plants ($\delta^{13}\text{C}_{\text{PLANT}}$) was calculated according to the model of Farquhar *et al.*
111 (1989) [eq.1] and depends on the $\delta^{13}\text{C}_{\text{ATM}}$ ($\delta^{13}\text{C}$ of the atmosphere) and on the ratio between
112 the $p\text{CO}_2$ inside the leaves and the atmospheric $p\text{CO}_2$ (c_i/c_a):

113

$$114 \text{ [eq.1] } \quad \delta^{13}\text{C}_{\text{PLANT}} = \delta^{13}\text{C}_{\text{ATM}} - a - (b - a) * c_i/c_a$$

115

116 where a is the fractionation during diffusion of the CO_2 from the atmosphere into leaves and
117 is fixed at 4.4‰; b is the fractionation during ribulose-1,5-bisphosphate
118 carboxylase/oxygenase (RuBisCO) carboxylation and has values of 26–30‰ (e.g. Farquhar *et*
119 *al.*, 1989; Arens *et al.*, 2000; Schubert and Jahren, 2012); and c_i/c_a is the ratio between
120 intercellular and atmospheric $p\text{CO}_2$. The c_i/c_a usually varies between 0.65 and 0.8 with a
121 maximum range between 0.3 and 0.9 (e.g. Farquhar *et al.* 1989; Arens *et al.*, 2000).

122

123 Post-photosynthetic fractionation also occurs during the biosynthesis of plant compounds,
124 which consequently have different $\delta^{13}\text{C}$ signatures (Badeck *et al.*, 2005). In general, non-

125 photosynthetic tissues are more ^{13}C -enriched by 1–3‰ than photosynthetic tissues such as
126 leaves (Cernusak *et al.*, 2009).
127
128 Studies suggested that the $\delta^{13}\text{C}_{\text{PLANT}}$ is primarily controlled by $\delta^{13}\text{C}_{\text{ATM}}$ (Arens *et al.*, 2000).
129 However, additional strong dependence of $\Delta^{13}\text{C}_\text{P}$ upon other factors complicates the $\delta^{13}\text{C}_{\text{PLANT}}$
130 - $\delta^{13}\text{C}_{\text{ATM}}$ relationship (e.g. Nordt *et al.*, 2016). The c_i/c_a ratio in [eq.1] is regulated by
131 stomatal conductance, which is governed by the closing or opening of the stomata. Stomatal
132 conductance can be influenced by many environmental factors, particularly water availability
133 and $p\text{CO}_2$. For example, Diefendorf *et al.* (2010) and Kohn (2010) showed that $\Delta^{13}\text{C}_\text{P}$ is
134 strongly correlated to mean annual precipitation (MAP) and plant functional types. Both these
135 studies found an increase of $\Delta^{13}\text{C}_\text{P}$ with increase of MAP. This dependence was modelled and
136 tested in the fossil record (Diefendorf *et al.*, 2015; Kohn, 2016). Schubert and Jahren (2012)
137 gave evidence that $\Delta^{13}\text{C}$ by C3 plants grown in environmentally controlled chambers
138 hyperbolically increases with increasing ambient $p\text{CO}_2$ levels. The model of Schubert and
139 Jahren (2012) was tested against ice-core records and used to reconstruct $p\text{CO}_2$ during the
140 Palaeocene–Eocene Thermal Maximum (PETM) (Schubert and Jahren 2013, 2015). In
141 contrast to this model, recent studies found no or negligible $p\text{CO}_2$ dependence over long time
142 scales (Kohn 2016), keeping open the question as to whether MAP or $p\text{CO}_2$ predominantly
143 control $\Delta^{13}\text{C}_\text{P}$. Moreover, Berner *et al.* (2000) and Beerling *et al.* (2002) experimentally
144 demonstrated an increase of plant $\Delta^{13}\text{C}$ with increase in $p\text{O}_2$ levels. Subsequently, Tappert *et*
145 *al.* (2013) proposed the use of fossil plant $\delta^{13}\text{C}$ to reconstruct palaeo- $p\text{O}_2$, assuming that, in
146 ambient air, plant $\Delta^{13}\text{C}$ is proportional to $p\text{O}_2$ and that physiological adaptations did not occur
147 through time. Although there is no agreement as to which factor is most important in
148 determining the carbon-isotope composition of modern plants, all these factors must be taken
149 into account to correctly interpret the carbon-isotope shifts registered by fossil plant material
150 in the geological record (Diefendorf *et al.*, 2010; Schubert and Jahren, 2012; Kohn, 2016).

151

152 **2.2 Modern and Cretaceous resin samples**

153

154 Modern resin samples from USA and New Caledonia were collected by A. R. Schmidt and L.
155 J. Seyfullah in 2005, 2010 and 2011 (USA) and in 2006 and 2011 (New Caledonia). J. Dal
156 Corso, G. Roghi and E. Ragazzi collected resins from different conifers growing at the
157 Botanical Gardens of the University of Padova in 2010. In Padova, *Araucaria heterophylla*
158 resin, leaves and wood were also collected at different heights from the base of the tree. Both
159 liquid-viscous and solid resins were sampled. Carbon-isotope data, plant species, altitude and
160 geographic provenance are summarized in Fig. 1 and Supplementary Table 1.

161

162 The Cretaceous amber analysed for this study derive from different deposits in Spain (25
163 samples), France (10 samples), and from the Grassy Lake deposit (5 samples) in Canada (Fig.
164 1). Their origin and ages are summarized in Supplementary Table 2 and Supplementary
165 Figure 1. Spanish amber samples were collected by X. Delclòs and are stored at Universitat
166 de Barcelona, Spain. They derive from several Aptian–Maastrichtian deposits from the
167 Central Asturian Depression, the West and East areas of the Basque-Cantabrian Basin, the
168 Maestrazgo (=Maestrat) Basin and the Castilian Platform. The age of these deposits is mainly
169 constrained by pollen and spores and includes uncertainties from ~1 up to ~18 Myrs (see
170 Table 2 and references therein; Peñalver & Delclòs, 2010; Barrón *et al.*, 2015). Samples of
171 French amber come from the collection of D. Néraudeau stored at the Université de Rennes,
172 France. The Late Albian-Early Cenomanian and Santonian ages of amber samples from
173 different localities in France are well constrained by pollen, spores, dinoflagellates,
174 foraminifers, ostracods and rudists (Peyrot *et al.*, 2005; Batten *et al.*, 2010), with uncertainties
175 of ~1 up to ~3 Myrs (see Table 2). Grassy Lake amber was collected and provided by A.
176 Wolfe (University of Alberta) and is Campanian in age, according to McKellar *et al.* (2008)

177 and Tappert *et al.* (2013). $\delta^{13}\text{C}_{\text{AMBER}}$ data of Cretaceous amber were coupled with previously
178 published $\delta^{13}\text{C}_{\text{RESIN}}$ data from Nissenbaum & Yakir (1995), Dal Corso *et al.* (2013) and
179 Tappert *et al.* (2013). The ages of some of these deposits, namely the Levantine amber from
180 Israel and Lebanon and the San Just amber from Spain, have been revised according to recent
181 stratigraphic data. The Lebanese amber-bearing deposits with bioinclusions (entrapped
182 fossilized organisms) are from the Lower Cretaceous: Ante-Jezzinian (Maksoud *et al.* 2014),
183 i.e., ante Lower Bedoulian (Bedoulian being Upper Barreman–Lower Aptian). Deposits of
184 Cretaceous Lebanese amber with bioinclusions are situated in the Chouf Sandstone Formation
185 (= Grès de Base or C1 in older usages), under the recently defined Jezzinian Regional-Stage
186 (uppermost Barremian–lower Aptian). The lower boundary of the Jezzinian is probably within
187 the uppermost Barremian (Maksoud *et al.* 2014). According to new biostratigraphical data,
188 the oldest Lebanese amber deposits with bioinclusions are Early Barremian and the youngest
189 are intra-Barremian (Maksoud *et al.*, 2016). The San Just amber outcrop is located in the
190 Maestrazgo Basin and is included in the Escucha Fm. of the Utrillas Group (SSS – Superior
191 Sedimentary Succession; Rodríguez-López *et al.*, 2009). It was dated as Middle-Upper Albian
192 by Villanueva-Amadoz *et al.* (2010), based on the palynological fossil record and it is now
193 constrained to the Upper Albian by comparison with similar deposits in the Basque–
194 Cantabrian Basin with similar fossil content (Barrón *et al.* 2015).

195

196 **2.3 $\delta^{13}\text{C}_{\text{RESIN}}$ analysis**

197

198 Clean sub-millimetric fragments of the collected modern resins were separated under the
199 microscope to perform $\delta^{13}\text{C}$ analysis. Close attention was paid in order to select clear resin
200 portions to avoid the presence of inclusions. The $\delta^{13}\text{C}$ analysis was performed on a Thermo
201 Scientific Delta V Advantage Isotope Ratio Mass Spectrometer in continuous flow mode,
202 coupled with a Flash 2000 Elemental Analyser and a ConFlo IV interface. 0.03–0.05 mg of

203 resin were weighed in a tin capsule and fed to the Elemental Analyser. The Mass
204 Spectrometer analysed CO₂ gas resulted from high temperature combustion. On the basis of a
205 long-term mean of >30 tin-cap analyses, a blank correction was applied to the raw data and
206 the results were calibrated against repeated analyses of IAEA-CH6 and IAEA-CH7
207 international standards, whose $\delta^{13}\text{C}$ is respectively -10.449‰ and -32.151‰ (Coplen *et al.*,
208 2006). The long-term internal reproducibility was estimated on repeated analyses of an
209 internal standard (C3 plant sucrose) and is better than 0.15‰ (1 σ).
210
211 Samples of Cretaceous amber were first crushed with an agate mortar to obtain a fine powder.
212 Repeated analyses on different portions of single Cretaceous amber specimens have shown
213 that the $\delta^{13}\text{C}$ is remarkably homogeneous within the same piece (Dal Corso *et al.*, 2013). We
214 thus consider the measured $\delta^{13}\text{C}$ as representative of the entire amber sample. The amber
215 powder was placed in a polypropylene tube and treated with 3M HCl to remove possible
216 residual carbonates from the sediments where the amber had been embedded. Samples were
217 then rinsed with deionized water until neutrality was reached and were oven-dried at 50°C.
218 1.5–2 mg of amber powder were weighed in tin capsules and fed into the Elemental Analyzer.
219 $\delta^{13}\text{C}$ analysis was performed using a Carlo Erba NA 1108 Elemental Analyzer coupled to a
220 SERCON Geo 20/20 IRMS running in continuous flow mode with a He carrier gas (flow rate
221 100ml per min). The reproducibility of the analyses was estimated using an internal standard
222 (alanine) routinely checked against international standards IAEA-CH-6 and IAEA-CH-7 and
223 traceable back to the VPDB standard. All results are accurate to better than $\pm 0.15\%$ (1 σ).
224

225 **2.4 Meta-analysis of terrestrial and marine carbon-isotope data**

226 The amber data generated in this study have been coupled with the published $\delta^{13}\text{C}_{\text{AMBER}}$ data
227 of Tappert *et al.* (2013), Nissenbaum & Yakir (1995) and Dal Corso *et al.* (2013), allowing
228 improved resolution of the $\delta^{13}\text{C}_{\text{AMBER}}$ record. To compare the variability of $\delta^{13}\text{C}_{\text{AMBER}}$ with

229 other Cretaceous C3 plant material we used the recently compiled ISOORG database (Nordt
230 *et al.*, 2016). ISOORG comprises $\delta^{13}\text{C}$ data ($\delta^{13}\text{C}_{\text{ISOORG}}$) of plant material including wood,
231 leaf, charcoal, coal, and bulk terrestrial organic matter from various geographical locations.
232 We also built a low-resolution wood $\delta^{13}\text{C}$ ($\delta^{13}\text{C}_{\text{WOOD}}$) record coupling the Lower Cretaceous
233 wood data extracted from ISOORG (Nordt *et al.*, 2016) with the Maastrichtian data of
234 Salazar-Jaramillo *et al.* (2016). Before processing data we excluded from ISOORG all
235 $\delta^{13}\text{C}_{\text{AMBER}}$ data, all of which were already included in our compilation. Some of the amber
236 deposits described here have age uncertainties of several millions of years, especially in the
237 case of the mid-Cretaceous Spanish ambers (Table 2 and Supplementary Figure 1). These
238 uncertainties depend on the fact that Cretaceous amber is commonly found in continental
239 (fluvial sediments, coal deposits) or coastal (brackish estuarine/lagoonal) deposits that lack
240 age-significant fossils. For this reason and to allow comparison with the ISOORG database,
241 $\delta^{13}\text{C}_{\text{AMBER}}$ data were placed into 5 Myrs-age bins following the criteria used by Nordt *et al.*
242 (2016). Amber with age uncertainty larger than the bin was excluded. The same procedure
243 was used also for $\delta^{13}\text{C}_{\text{WOOD}}$ from Salazar-Jaramillo *et al.* (2016). Box-and-whiskers plots for
244 $\delta^{13}\text{C}_{\text{AMBER}}$, $\delta^{13}\text{C}_{\text{WOOD}}$ and $\delta^{13}\text{C}_{\text{ISOORG}}$ data were built for each age bin with a sample size of at
245 least 5 (Krzywinski and Altman, 2014). To compare the terrestrial $\delta^{13}\text{C}$ signal to the marine
246 $\delta^{13}\text{C}$ signal we took marine carbonate data from the database compiled by Prokoph *et al.*
247 (2008) and Bodin *et al.* (2015). We used $\delta^{13}\text{C}$ and $\delta^{18}\text{O}$ data from benthic and planktonic
248 foraminifera and belemnites. Terrestrial $\delta^{13}\text{C}$ data were also compared to the $\delta^{13}\text{C}_{\text{ATM}}$, which
249 was estimated from the $\delta^{13}\text{C}$ and $\delta^{18}\text{O}$ of benthic foraminifera using the equations proposed
250 by Tipple *et al.* (2010). A third-degree polynomial curve was fitted to the data to compare the
251 terrestrial and marine carbonate $\delta^{13}\text{C}$ records. Prediction intervals for individual observations
252 hold about 95% of data. Polynomial curve fitting by the least-squares method and prediction
253 intervals were obtained with JMP software, version 10 (SAS Institute Inc., Cary, NC, USA).
254

255 **3. RESULTS**

256

257 **3.1 Modern resin $\delta^{13}\text{C}$**

258

259 The $\delta^{13}\text{C}$ of all the analysed modern resins varies from -31.6‰ to -22.8‰ (mean \pm SD = -
260 26.7 \pm 1.8‰, n=84; Table 1). $\delta^{13}\text{C}_{\text{RESIN}}$ values obtained in this study show a normal distribution
261 with a mean of -26.7‰ (Fig. 2). The mean $\delta^{13}\text{C}_{\text{RESIN}}$ is more ^{13}C -enriched than the mean
262 global leaf $\delta^{13}\text{C}$ (-28.5‰ calculated from data of Diefendorf *et al.*, 2010; Fig. 3A). A
263 statistically significant difference (p value = 0.001) exists between liquid-viscous resin and
264 solid resin, the former having more ^{13}C -enriched values (mean -25.9‰) than the latter (mean -
265 27.1‰) (Fig. 3A). Resin has $\delta^{13}\text{C}$ values systematically more ^{13}C -enriched by 1–2.3‰ than
266 those of bulk leaf and wood samples collected from the same branch at the same tree height in
267 *Araucaria heterophylla*, *Picea abies* and *Cupressus arizonica* (Fig. 3B). Resin, wood and
268 leaves collected from a single tree of *Araucaria heterophylla* at different heights also possess
269 variable $\delta^{13}\text{C}$ signatures (Fig. 3C). Differences of up to 6‰ exist between the mean $\delta^{13}\text{C}$ of
270 resins from different plant species (Table 1). The $\delta^{13}\text{C}_{\text{RESIN}}$ from different tree genera growing
271 at the same altitude in the same locality (Padova, Italy) differs by about 2–5‰ (Fig. 3B).
272 Liquid-viscous and solid resin $\delta^{13}\text{C}$ of *Pinus* and *Araucaria* significantly increases with
273 increasing altitude of the sampling site (Fig. 4; liquid-viscous resin, $R = 0.527$, p value <
274 0.001; Solid resin of *Pinus* and *Araucaria*, $R = 0.603$, p value < 0.001). Similar correlation
275 was also observed between $\delta^{13}\text{C}_{\text{LEAF}}$ and altitude ($R=0.59$; Körner *et al.*, 1988). The $\delta^{13}\text{C}_{\text{RESIN}}$
276 values for the most represented genera show that *Pinus* resin is statistically indistinguishable
277 from *Araucaria* resin (p value = 0.6, Students' t -test; Table 1).

278

279 **3.2 Cretaceous amber $\delta^{13}\text{C}$**

280

281 The $\delta^{13}\text{C}$ of amber from Spain varies between -17‰ and -24.2‰ (mean = $-20.1 \pm 1.8\text{‰}$) in the
282 range expected for C3 plant resins (Table 2). Similarly, $\delta^{13}\text{C}$ of amber from France and
283 Canada ranges from -18.5‰ to -23.5‰ (mean = $-21.1 \pm 1.9\text{‰}$) and from -21.4‰ to -23.4‰
284 (mean = $-22.7 \pm 0.8\text{‰}$), respectively (Table 2). The compiled Cretaceous amber and ISOORG
285 $\delta^{13}\text{C}$ values show a normal distribution (Fig. 5A). On average, amber is more ^{13}C -enriched
286 (mean = $-22.3\text{‰} \pm 1.9\text{‰}$) than Cretaceous C3 plant material (mean = $-24.2\text{‰} \pm 1.3\text{‰}$) and
287 wood (mean = $-23.1\text{‰} \pm 1.3\text{‰}$) (Fig. 5B). Cretaceous $\delta^{13}\text{C}_{\text{AMBER}}$ data are more dispersed than
288 $\delta^{13}\text{C}$ values of C3 plant material: the box-and-whisker plots (Fig. 5B) show the interquartile
289 range (IQR) of $\delta^{13}\text{C}_{\text{AMBER}}$ to be much larger (2.5‰ , Table 2) than $\delta^{13}\text{C}_{\text{ISOORG}}$ (1.4‰). F-test
290 for the equality of variances indicates that the variances of $\delta^{13}\text{C}_{\text{AMBER}}$ and $\delta^{13}\text{C}_{\text{ISOORG}}$ are
291 significantly different ($p < 0.0001$). SD and IQR were calculated for each age bin (Table 2)
292 and show that $\delta^{13}\text{C}_{\text{AMBER}}$ is generally more dispersed than the $\delta^{13}\text{C}_{\text{ISOORG}}$ and $\delta^{13}\text{C}_{\text{WOOD}}$.
293 Amber, wood and ISOORG data show that latest Cretaceous (Maastrichtian) $\delta^{13}\text{C}$ values are
294 more ^{13}C -depleted than those of the Early Cretaceous (Hauterivian–Barremian) by $2.5\text{--}3\text{‰}$
295 (Fig. 6). The marine $\delta^{13}\text{C}$ record from whole rock, belemnite, and foraminifera (Prokoph *et*
296 *al.*, 2007; Bodin *et al.*, 2015) shows a pattern that only partially matches the terrestrial records
297 (Fig. 6). The $\delta^{13}\text{C}_{\text{ATM}}$ calculated from benthic foraminifera shows a decrease of approx. 1‰
298 from the Aptian to the Maastrichtian that mirrors the decrease ($2.5\text{--}3\text{‰}$) shown by terrestrial
299 plants (Fig. 7).

300

301 4. DISCUSSION

302

303 4.1 Modern resin

304

305 4.1.2 Effect of resin hardening on the $\delta^{13}\text{C}_{\text{RESIN}}$

306

307 To obtain reliable information on the physiology of plants and the environmental conditions
308 under which they grow from the carbon-isotope geochemistry of resin, it is necessary to
309 understand whether the measured $\delta^{13}\text{C}_{\text{RESIN}}$ values actually represent the pristine composition
310 at the time of resin biosynthesis. After exudation, resin is composed of up to 50% of volatile
311 fraction (mainly monoterpenes and sesquiterpenes). The volatile fraction is lost rapidly on
312 exposure of resin to air and sunlight, whereas the non-volatile fraction (mainly diterpene acids
313 in conifer resin) undergoes polymerization (cross-linking and isomerization) with the
314 formation of high-molecular-weight polymers (Langenheim, 1990; Scalarone *et al.*, 2003;
315 Lambert *et al.*, 2008; Ragazzi and Schmidt, 2011). This selective removal of moieties points
316 to a possible change of the bulk $\delta^{13}\text{C}_{\text{RESIN}}$ during resin hardening (Dal Corso *et al.*, 2011). Our
317 dataset comprises both liquid–viscous resins sampled shortly after exudation and solid resins
318 that already had hardened at the site of exudation. A statistically significant difference ($p =$
319 0.001) is observed between liquid–viscous (mean = -25.9‰) and solid resin (-27.1‰), with
320 an overall 1.2‰ ^{13}C -enriched values in the former (Fig. 3A). We conclude that volatile mono-
321 and sesquiterpenes released by resin during hardening are more ^{13}C -enriched than the non-
322 volatile diterpenoid and triterpenoid acids. Consequently, changes in the pristine $\delta^{13}\text{C}_{\text{RESIN}}$
323 occur soon after resin exudation. Future organic geochemical studies should precisely
324 determine the magnitude of these isotopic changes in different resin types by studying the
325 pattern of volatile loss during hardening, and the specific carbon-isotope signature and the
326 relative abundance of the different resin compounds. Such a study would probably allow
327 correction of the measured $\delta^{13}\text{C}$ of solid resin back to the pristine signature at the time of
328 exudation in order to faithfully interpret the data.

329

330 **4.1.2 Differences between the $\delta^{13}\text{C}_{\text{RESIN}}$ and the $\delta^{13}\text{C}$ of other plant tissues**

331

332 Post-photosynthetic fractionation in plants results in differences in the $\delta^{13}\text{C}$ of plant tissues
333 (Badeck *et al.*, 2005). In general, non-photosynthetic tissue tends to be more ^{13}C -enriched
334 than photosynthetic tissue: leaves were found to have isotopically lighter values than wood
335 and roots, and above-ground organs are more ^{13}C -depleted than below-ground material
336 (Badeck *et al.*, 2005; Cernusak *et al.*, 2009). Several biochemical causes have been invoked to
337 explain this widespread isotopic behaviour and are still a topic of debate (review by Cernusak
338 *et al.*, 2009).

339

340 $\Delta^{13}\text{C}_\text{P}$ during resin biosynthesis is evident from our data when comparing the $\delta^{13}\text{C}_\text{RESIN}$ with
341 the $\delta^{13}\text{C}$ of other plant tissues. Our dataset shows that the mean $\delta^{13}\text{C}_\text{RESIN}$ of fresh liquid-
342 viscous resin (-25.9‰) is more ^{13}C -enriched by 2.6‰ than the mean $\delta^{13}\text{C}_\text{LEAF}$ from a
343 published compilation of data of C3 leaves (-28.5‰; Fig. 3A, Diefendorf *et al.*, 2010), as
344 expected from a non-photosynthetic plant compounds. Solid resin (-27.1‰), as previously
345 described, is more ^{13}C -depleted than liquid-viscous resin, but remains more ^{13}C -enriched than
346 mean leaf $\delta^{13}\text{C}$, so that carbon-isotope changes due to hardening do not overshadow post-
347 photosynthetic $\Delta^{13}\text{C}_\text{P}$ between resin and leaf. This difference is also evident from samples
348 taken from the same trees and branches. Solid resin of *Araucaria heterophylla*, *Picea abies*
349 and *Cupressus arizonica* sampled at the Botanical Garden in Padova (Italy) has higher $\delta^{13}\text{C}$
350 values than leaves from the same branch by approx. 1–2‰ (Fig. 3B and C). This difference
351 should be corrected for the loss of volatiles and was likely larger by 1–2‰ at the time of resin
352 exudation (see 4.1.1).

353

354 Similar differences exist also between resin and wood $\delta^{13}\text{C}$ signatures. In *Picea abies* and
355 *Araucaria heterophylla*, resin is more ^{13}C -enriched than wood, which, in turn, shows very
356 small $\delta^{13}\text{C}$ differences compared to leaf carbon-isotope signatures (Fig. 3B and C). As shown
357 by the trees sampled for this study, fractionation during resin biosynthesis does occur and

358 results in a very ^{13}C -enriched $\delta^{13}\text{C}_{\text{RESIN}}$ signature (by approx. 2–4‰) when compared to the
359 $\delta^{13}\text{C}$ of other organs from the same plant branch. On the contrary, $\delta^{13}\text{C}_{\text{WOOD}}$ and $\delta^{13}\text{C}_{\text{LEAF}}$
360 show little difference (<1‰) within the same branch (Fig. 3B and C). Other studies show that
361 on average stem wood and roots are more ^{13}C -enriched by 1–1.9‰ than is leaf material
362 (Badeck *et al.*, 2009). Our results suggest that the post-photosynthetic $\Delta^{13}\text{C}_\text{P}$ is larger for resin
363 than for other bulk plant tissues. Such patterns are visible also after resin hardening, meaning
364 that both volatile (monoterpenes and sesquiterpenes), and non-volatile (diterpene acids) are
365 affected.

366

367 **4.1.3 Environmental and physiological effects on $\delta^{13}\text{C}_{\text{RESIN}}$**

368

369 Our results show that the carbon-isotope signature of resin records the environmental and
370 physiological effects of C3 plant ^{13}C discrimination, as do other plant tissues. The $\delta^{13}\text{C}_{\text{RESIN}}$
371 varies by up to 2‰ within the same tree (Fig. 3C) and on average $\delta^{13}\text{C}_{\text{RESIN}}$ differs by up to
372 6‰ between plant species and genera, and between different localities (Table 1 and
373 Supplementary Table 1). This high variability in resin carbon-isotope composition is likely
374 related to the local climatic and growing conditions, and plant physiology that regulate ^{13}C
375 discrimination in plants [eq. 1].

376

377 Several studies have explored the dependence of plant ^{13}C discrimination in response to
378 environmental gradients, which control the stomatal aperture and thus determine the c_i/c_a in
379 [eq. 1] (see Cernusak *et al.*, 2013 for a summary). As previously described, C3 plants
380 fractionate carbon isotopes depending on a number of factors: mean annual precipitation,
381 $p\text{CO}_2$, soil moisture, nutrient availability, irradiation, etc., and can explain most of the $\delta^{13}\text{C}$
382 variability of plant biomass (e.g. Diefendorf *et al.*, 2010; Kohn, 2010; Schubert and Jahren,
383 2012; Cernusak *et al.*, 2013). Here we consider the variability of $\delta^{13}\text{C}_{\text{RESIN}}$ within the same

384 tree, with altitude of the growing site and between plant species, and show that $\delta^{13}\text{C}_{\text{RESIN}}$
385 varies in ways that are similar to other tissues depending on the environmental conditions
386 under which the plant grew.

387

388 Solid resin $\delta^{13}\text{C}$ varies within an individual *Araucaria heterophylla* by approx. 2‰
389 (depending on different heights along the trunk), as also observed for leaf and wood $\delta^{13}\text{C}$
390 (Fig. 3C). This difference suggests that either seasonality and/or physiological factors can
391 considerably change the $\delta^{13}\text{C}_{\text{RESIN}}$ within an individual plant. This phenomenon has also been
392 observed in leaf $\delta^{13}\text{C}$, which varies by approx. 1–4‰ along vertical canopy profiles among
393 conifers (e.g. Duursma and Marshall, 2006 and references therein). $\delta^{13}\text{C}_{\text{LEAF}}$ generally
394 increases from the bottom to the top of the crown due to hydraulic conductance or irradiation
395 variations (Koch *et al.*, 2004; Duursma and Marshall, 2006; Cernusak *et al.*, 2013). Our resin,
396 leaf and wood $\delta^{13}\text{C}$ data from *Araucaria heterophylla* appear to show a similar pattern (Fig.
397 3C).

398

399 The $\delta^{13}\text{C}$ of fresh liquid–viscous resin (Fig. 4A) increases with altitude from sea level to
400 3050m (Fig. 4B). This effect is also evident by plotting solid and liquid–viscous resin of
401 *Pinus* and *Araucaria*, the most representative genera. In both cases $\delta^{13}\text{C}_{\text{RESIN}}$ increases
402 linearly with altitude ($p < 0.001$; Fig. 4). These results contradict a previous study on
403 $\delta^{13}\text{C}_{\text{RESIN}}$, which found a general ^{13}C -depletion along altitudinal transects in the UK to a
404 maximum altitude of 550m (Stern *et al.*, 2008). The dataset of $\delta^{13}\text{C}_{\text{RESIN}}$ values presented in
405 this study comprises a sample from altitudes up to approx. 3000m and is more comparable to
406 the existing $\delta^{13}\text{C}$ data from C3 leaves and wood from localities around the world of altitudes
407 up to 5600m (Körner *et al.*, 1988; Warren *et al.*, 2001). Decreasing ^{13}C discrimination with
408 altitude has been extensively observed in conifer leaves and wood (e.g. Körner *et al.*, 1988;
409 Hultine and Marshall, 2000; Warren *et al.*, 2001; Cernusak *et al.*, 2013). The net effect of

410 altitude on plant $\delta^{13}\text{C}$ is, however, considered negligible compared, for example, to MAP
411 (Kohn, 2016). Indeed, the mechanism by which the discrimination-altitude correlation
412 operates is unclear: many authors have invoked changes in leaf morphology, water
413 availability, leaf nitrogen content, temperature, decrease of $p\text{CO}_2$ with elevation, $p\text{O}_2$ and
414 irradiance as possible causes (e.g. Hultine and Marshall, 2000; Diefendorf *et al.*, 2010;
415 Cernusak *et al.*, 2013). The strong dependence of plant $\delta^{13}\text{C}$ towards very different
416 environmental factors (e.g. Arens *et al.*, 2000; Diefendorf *et al.*, 2010), points to a possible
417 combined effect of these factors on $\delta^{13}\text{C}_{\text{RESIN}}$ with altitude. Additional $\delta^{13}\text{C}_{\text{RESIN}}$ analyses
418 along altitudinal transects coupled with precise data about the environmental conditions
419 (moisture levels, temperature, irradiance, etc.) will elucidate the $\delta^{13}\text{C}_{\text{RESIN}}$ -altitude correlation
420 found in this study and permit a greater understanding of the relative contribution of these
421 effects on the final carbon-isotope signature of the resin. The significant correlation between
422 $\delta^{13}\text{C}_{\text{RESIN}}$ and altitude, similar to the correlation found using other plant substrates, means that
423 environmental effects on plant $\Delta^{13}\text{C}$ are recorded by resin despite fractionation during
424 biosynthesis, which determines the differences between its $\delta^{13}\text{C}$ and that of other tissues (Fig.
425 3B and C), and during hardening (Fig. 3).

426

427 Several authors have reported high $\delta^{13}\text{C}$ variability (e.g. up to 6‰ in lowland rainforest
428 stands; Bonal *et al.*, 2000) among plant species under the same environmental conditions (e.g.
429 Leavitt and Long, 1986; Zhang and Cregg, 1996; Schubert and Cui, 2016 and references
430 therein). These inter-specific differences in the $\delta^{13}\text{C}$ of plants are related to differences in
431 $\Delta^{13}\text{C}$ regulated by the morphology of leaf and stomata that control efficiency of water use and
432 the c_i/c_a ratio (Murray *et al.*, 1998). The $\delta^{13}\text{C}$ of resins sampled at the same altitude in the
433 same locality (Padova, Italy) from different tree genera differs by about 2–5‰ (Fig. 3B).

434 Overall, the $\delta^{13}\text{C}_{\text{RESIN}}$ varies by up to 6‰ between plant species (Table 1). These findings
435 suggest that variations in ^{13}C discrimination linked to plant physiology are recorded also by

436 resin. Interestingly, when resins are grouped at a high taxonomic level, the $\delta^{13}\text{C}$ differences
437 are not statistically significant ($p = 0.598$) and their mean calculated $\delta^{13}\text{C}_{\text{RESIN}}$ values
438 (*Araucaria* = -27.1‰ ; *Pinus* = -26.9‰) approach that of the mean of our worldwide resin
439 samples.

440

441 **4.2 Cretaceous $\delta^{13}\text{C}_{\text{AMBER}}$ data**

442 As hypothesised in the introduction, amber could potentially be used to reconstruct the
443 carbon-isotope composition of the palaeoatmosphere, as is the case with other plant tissues
444 such as leaf and wood. Our data on modern material show that the $\delta^{13}\text{C}_{\text{RESIN}}$ can record
445 changes in ^{13}C discrimination by C3 plants as seen in leaves and wood. Records of the $\delta^{13}\text{C}$
446 from fossil wood and bulk leaves or cuticles, despite their natural variability within each
447 stratigraphic interval, parallel those of marine carbonates and can record global long- and
448 short-term perturbations of the carbon cycle (e.g. Gröcke *et al.*, 1999; Gröcke, 2002; Dal
449 Corso *et al.*, 2011). It is therefore reasonable to expect amber to record the same carbon-
450 isotope changes. In the following sections we will discuss the potential of amber as a
451 chemostratigraphic tool and as a proxy for Cretaceous palaeoatmosphere in the light of
452 present-day resin carbon-isotope geochemistry.

453

454 **4.2.1 Carbon-isotope signature of Cretaceous amber vs other C3 fossil plant material: 455 pristine differences and diagenetic effects**

456

457 On average, Cretaceous $\delta^{13}\text{C}_{\text{AMBER}}$ (mean = $-22.3\text{‰} \pm 1.9\text{‰}$) is ^{13}C -enriched by 1.6‰ ($p <$
458 0.0001) relative to other C3 plant material (mean = $-24.2\text{‰} \pm 1.3\text{‰}$) and wood (mean = -
459 $23.1\text{‰} \pm 1.3\text{‰}$) (Fig.5). Amber is always more ^{13}C -enriched than wood by $1.5\text{--}2\text{‰}$ for each
460 age bin present here (Table 2, Fig. 6). A similar offset was also observed for Upper Triassic
461 conifer amber and wood from Italy ($+2.5\text{‰}$) (Dal Corso *et al.*, 2011), and for Upper

462 Cretaceous gymnosperm-derived coals and associated resinites from Australia (+2.6‰)
463 (Murray *et al.*, 1998). A recent compilation of plant $\delta^{13}\text{C}$ data for all the Phanerozoic shows
464 amber is on average the most ^{13}C -enriched plant tissue (Nordt *et al.*, 2016). The differences
465 between resin and plant tissues (leaf and wood) observed in our modern material (Fig. 3) can
466 explain amber ^{13}C -enriched values, showing that fossil material can retain the same patterns
467 observed in modern samples, that is, with the differences being generated by fractionation
468 during resin biosynthesis. Moreover, the dispersion of $\delta^{13}\text{C}$ data is larger in amber (SD =
469 1.95‰; IQR = 2.5‰) than in other C3 plant material (SD = 1.31‰; IQR = 1.4‰) (Table 2).
470 This difference is evident also when considering separately different plant tissues with a
471 sample size similar to the size of our amber database and with the same age. In general, amber
472 $\delta^{13}\text{C}$ values are more scattered than those of Cretaceous wood (SD = 1.31‰; IQR = 1.47‰),
473 charcoal (SD = 1.55‰; IQR = 2‰) and coal (SD = 1.43‰; IQR = 1.23‰). In the
474 Hauterivian–Barremian (age bin = 130 Ma) and Maastrichtian (age bin = 70 Ma) $\delta^{13}\text{C}_{\text{AMBER}}$
475 has a greater spread in values than wood $\delta^{13}\text{C}$; and in the Turonian (90 Ma) and in the
476 Maastrichtian (70 Ma) the amber carbon-isotope signature is more variable than in other plant
477 substrates (Fig. 6; Table 2).
478
479 Comparison with modern material (Fig. 5B) points to an original high plant $\delta^{13}\text{C}$ variability
480 for amber but less in other fossil plant remains (Dal Corso *et al.*, 2011). Taphonomical and
481 diagenetic processes could enhance the original $\delta^{13}\text{C}$ discrepancies between tissues and
482 accentuate the spread in $\delta^{13}\text{C}$ data. The carbon-isotope signature of plant tissue changes
483 towards more negative values during diagenesis (Spiker & Hatcher, 1987), a fact also
484 confirmed here for conifer resin (Fig. 3A). As previously discussed (section 4.1.2), solid resin
485 becomes more depleted by 1.2‰ when altered from fresh liquid–viscous resin, probably
486 because of the loss of ^{13}C -rich volatiles during hardening (Fig. 3A). Subsequently, resin
487 maturation causes polymerization of non-volatile components accompanied by cross-linking

488 and isomerization, but no significant diagenetic changes of the carbon-isotope composition
489 take place (Dal Corso *et al.*, 2013; Tappert *et al.*, 2013). In support of this assumption, Dal
490 Corso *et al.* (2013) observed that altered and unaltered areas within the same Lower
491 Cretaceous amber pieces from the San Just deposit show no $\delta^{13}\text{C}$ differences despite oxidation
492 and degradation, as revealed by infra-red spectroscopic and thermogravimetric analyses. This
493 observation indicates that amber is a closed system with respect to C-isotopes as soon as it
494 hardens. By contrast, other plant remains can experience a more pervasive diagenetic
495 overprint. Charcoalification and coalification can severely change the pristine $\delta^{13}\text{C}$ of tissues
496 (e.g. Gröcke, 1998; Yans *et al.*, 2010 and references therein). Pyrolysis experiments have
497 shown the $\delta^{13}\text{C}$ of wood to become either more ^{13}C -enriched or depleted depending on the
498 temperature of combustion reached (Jones and Chaloner, 1991; Hall *et al.*, 2008). Upon
499 burial, the preferential degradation of hemicellulose (average $\delta^{13}\text{C}$ of about -23‰) and
500 cellulose (average $\delta^{13}\text{C}$ of about -25‰) over lignin (average $\delta^{13}\text{C}$ of about -28‰) can change
501 the pristine bulk wood $\delta^{13}\text{C}$ by several ‰ towards more negative values (e.g. Spiker &
502 Hatcher, 1987; van Bergen and Poole, 2002). As pointed out by Dal Corso *et al.* (2011), these
503 diagenetic processes could be responsible not only for changing the average $\delta^{13}\text{C}$ of plant
504 tissue but also for narrowing $\delta^{13}\text{C}$ variability of Triassic fossil wood and leaves compared
505 with amber. Similarly, the Cretaceous $\delta^{13}\text{C}_{\text{AMBER}}$ is consistently more variable than the $\delta^{13}\text{C}$ of
506 other plant substrates (Fig. 5 and 6, Table 2). Despite these complicating factors, data show
507 that amber is very resistant to diagenesis and can preserve the pristine carbon-isotope
508 signature of resin better than other plant tissues and, consequently, can retain information
509 about past environments and climate.

510

511 **4.2.2 Interpreting $\delta^{13}\text{C}_{\text{AMBER}}$ record through the Cretaceous and comparison with**
512 **terrestrial organic matter and marine carbonate carbon-isotope records**

513

514 Excluding the Barriasian–Valanginian interval for which the $\delta^{13}\text{C}_{\text{AMBER}}$ data available are
515 indeed very scarce, the most remarkable feature shown by the Cretaceous $\delta^{13}\text{C}_{\text{AMBER}}$ record is
516 an approx. 2.5‰ negative trend from the Hauterivian–Barremian (130 Ma) to the
517 Maastrichtian (70 Ma). Similarly, Late Cretaceous wood $\delta^{13}\text{C}$ is more ^{13}C -depleted than Early
518 Cretaceous wood $\delta^{13}\text{C}$ (Fig. 6). Maastrichtian C3 plant $\delta^{13}\text{C}$ data from ISOORG compiled by
519 Nordt *et al.*, 2016 (various types of fossil C3 plant remains minus amber data) are
520 approximately 3‰ more ^{13}C -depleted than the Hauterivian–Barremian $\delta^{13}\text{C}$ data (Fig. 6). In
521 the earliest Cretaceous, ISOORG $\delta^{13}\text{C}$ rises from the Jurassic–Cretaceous boundary to the
522 early Albian (125 Ma). The $\delta^{13}\text{C}$ changes shown by ISOORG, wood, and amber records
523 during the Cretaceous are very similar to or smaller than their carbon-isotope variability
524 within each age bin (Table 2 and Fig. 6). Moreover, the resolution of the data is very low and
525 long intervals of the Cretaceous are not covered. This drawback obviously hampers a correct
526 interpretation of the trends because the non-homogeneous distribution of data through time
527 biases the fitting. However, the overall 2.5–3‰ negative depletion towards the end of the
528 Cretaceous is in clear agreement among the global compilation of plant substrates. On the
529 contrary, the marine carbonate carbon-isotope records seem only to partially parallel the
530 terrestrial long-term signal. In the Early Cretaceous belemnite $\delta^{13}\text{C}$ record, a long-term
531 positive trend from the late Berriasian–early Valanginian to the middle Aptian is followed by
532 a long-term negative trend, which ends in the middle Albian (Prokoph *et al.*, 2008; Bodin *et*
533 *al.*, 2015). For subsequent intervals, belemnite $\delta^{13}\text{C}$ data are sparse but become overall more
534 ^{13}C -enriched in the Late Cretaceous (Fig. 6). Data from planktonic and benthic foraminifera
535 are available only from the early Albian onwards: $\delta^{13}\text{C}$ declines by approx. 1‰ from the early
536 Albian to the Albian–Cenomanian boundary then rises by the same magnitude until the
537 Cenomanian–Turonian boundary and remains stable until the end of the Cretaceous (Fig. 6;
538 Prokoph *et al.*, 2008). The schematic curve of whole-rock carbonate $\delta^{13}\text{C}$ analyses compiled
539 by Erba *et al.* (2004) mirrors the belemnite and foraminiferal records (Fig. 6). Despite the

540 offset in the carbon-isotope signature of the different proxies, which depends on the water
541 mass in which the carbonate was precipitated or secreted (Prokoph *et al.*, 2008), marine
542 carbonates show the same general carbon-isotope trends during the Cretaceous (Fig. 6). Using
543 the equation proposed by Tipple *et al.* (2010), we calculated the $\delta^{13}\text{C}$ of the Cretaceous
544 atmosphere ($\delta^{13}\text{C}_{\text{ATM}}$) from the available $\delta^{13}\text{C}$ data of benthic foraminifera compiled by
545 Prokoph *et al.* (2008). The polynomial curve fitted to the inferred $\delta^{13}\text{C}_{\text{ATM}}$ data points shows a
546 small long-term decline from approx. 125 Ma to the end of the Cretaceous (Fig. 7). The
547 $\delta^{13}\text{C}_{\text{ATM}}$ trend seems to mimic the 2.5–3‰ negative trend described by C3 plant material,
548 although with much smaller magnitude (1‰) (Fig. 7). This general relationship suggests that
549 $\delta^{13}\text{C}$ from Cretaceous amber and other plant tissues, despite high variability within each age
550 bin, can record changes in the carbon-isotope composition of the atmosphere. The relatively
551 small atmospheric shift, however, cannot alone explain the changes in plant $\delta^{13}\text{C}$
552 records. These data, however, also suggest $\Delta^{13}\text{C}_{\text{P}}$ increased towards the end of the Cretaceous
553 along with decreasing $\delta^{13}\text{C}_{\text{ATM}}$ values. It is thus necessary to account for changes in climate
554 and floral community structure, upon which plant $\Delta^{13}\text{C}$ is strongly dependent, to faithfully
555 interpret Cretaceous plant $\delta^{13}\text{C}$ data (e.g. Diefendorf *et al.*, 2010; Schubert and Jahren, 2013).
556
557 Given the different provenances of Cretaceous amber, some of the changes in its $\delta^{13}\text{C}$ through
558 time and the large variability within each age bin (Fig. 6) can be attributed to local plant
559 growing conditions, which are hardly constrainable for amber deposits, given the fact that
560 amber is rarely found *in situ* and is mostly reworked. The altitude of the Cretaceous resin-
561 producing trees, seemingly an important control on modern resin carbon-isotope signature
562 (see section 3), is relatively well known for those examples situated close to former sea level,
563 namely the Albian amber deposits (Peñacerrada, El Soplao), Albian-Cenomanian amber
564 deposits (Archingeay-Les Nouillers, Cadeuil, Fouras, Ile d'Aix, La Buzinie: Néraudeau *et al.*,

565 2009; Girard *et al.*, 2008) and the Santonian amber deposits (Belcodène, Piolenc: Gomez *et*
566 *al.*, 2003; Saint-Martin *et al.*, 2013). However, for other deposits the palaeo-altitude is
567 unknown and presumably variable. The depleted $\delta^{13}\text{C}$ values of Campanian amber from
568 Canada could be partially related to a particularly high palaeo-latitude location of the
569 deposits (Fig. 1) and possibly from a different climatic regime (see compilation by Scotese
570 2002). Insect infestation has been shown to have substantially ^{13}C -enriched the $\delta^{13}\text{C}$ of part of
571 the Turonian New Jersey ambers analysed by McKellar *et al.* (2011), which are also included
572 in our dataset (Fig. 6). At a micro-environmental scale, the height at which the Cretaceous
573 amber was produced within the tree trunk is impossible to determine, and this factor has been
574 previously shown to affect the $\delta^{13}\text{C}$ of modern resin by several ‰ (see section 3). Different
575 fractionation pathways of different plant functional type through time could also be
576 responsible for the $\delta^{13}\text{C}_{\text{AMBER}}$ changes (Diefendorf *et al.*, 2010). In fact, the species
577 composition responsible for the amber production differed through the Cretaceous, even
578 though the number of species remained the same (1–2) for each time interval (see, e.g.,
579 Tappert *et al.*, 2013; Nohra *et al.*, 2015). As previously described, modern $\delta^{13}\text{C}_{\text{RESIN}}$ varies by
580 up to 6‰ between plant species from different localities (Table 1), and the $\delta^{13}\text{C}$ of resins
581 sampled in the same locality from different tree species differs by about 2–5‰ (Fig. 3B). To
582 avoid this problem it is recommended to use a plant substrate that averages the inter-specific
583 carbon-isotope differences for palaeo-atmosphere reconstructions (e.g. Arens *et al.*, 2000).
584
585 Significantly, the Cretaceous Period was a time of rapid taxonomic diversification and
586 ecological radiation of Angiosperms, starting from the Aptian–Albian and continuing to the
587 Campanian (McElwain *et al.*, 2005). Angiosperm tissue $\delta^{13}\text{C}$ is generally more depleted than
588 conifer tissue $\delta^{13}\text{C}$ (Arens *et al.*, 2000; Diefendorf *et al.*, 2010), something reflected in the
589 isotopic composition of modern resin (Murray *et al.*, 1998). The decline in the carbon-isotope
590 composition of plant material, of which the botanical affinity is unknown, from the Early to

591 the latest Cretaceous (Fig. 6) could be related to an increase in the relative abundance of
592 Angiosperms. This factor could lie behind the ISOORG trends, where tissues from different
593 sources are lumped together (charcoal, coal, leaf, wood and bulk terrestrial organic matter),
594 but Cretaceous amber considered in this study comes only from conifers (e.g. Tappert *et al.*,
595 2013). Therefore, micro-environmental conditions, different plant functional type
596 discrimination, and diagenesis (see 4.2.1) are all factors that could have modified the
597 Cretaceous plant $\delta^{13}\text{C}$ signature and determined the high variability for each age bin, but such
598 factors are difficult to constrain for the fossil record and thus their relative effect on plant $\delta^{13}\text{C}$
599 cannot be calculated. On the other hand, the similar general long-term $\delta^{13}\text{C}$ patterns shown by
600 ISOORG, wood, and amber suggest there is a global dominant factor that regulated plant
601 discrimination throughout the long time scale of the Cretaceous (from 145 Ma to 66 Ma;
602 Gradstein *et al.*, 2012).

603

604 Today, MAP accounts for more than the 50% of the variations observed in plant $\Delta^{13}\text{C}$,
605 implying that stomatal conductance (c_i/c_a in eq.1) is primarily driven by water availability:
606 The $\Delta^{13}\text{C}_p$ increases with increasing MAP (Diefendorf *et al.*, 2010; Kohn 2010). Diefendorf *et*
607 *al.* (2015) shows that $\Delta^{13}\text{C}_p$ in Palaeogene plants responded to water availability in a way
608 similar to modern plants. MAP calculated from compact-corrected depth to calcic horizon in
609 palaeosols in the Colorado Plateau (Retallack, 2009) indicates Late Cretaceous MAP was
610 higher (approx. 600–650 mm on average) than the Early Cretaceous MAP (approx. 450 mm
611 on average) in the study area (Fig. 7). According to the general $\Delta^{13}\text{C}_p$ –MAP relationship
612 calculated for modern leaves (Diefendorf *et al.*, 2010), such increase of MAP would increase
613 the $\Delta^{13}\text{C}_p$ by approx. 1–2‰. Consequently, plant carbon-isotope composition would become
614 more ^{13}C -depleted, suggesting that Cretaceous plant $\delta^{13}\text{C}$ data record changes in the global
615 hydrological cycle, as predicted by the relationships found by Diefendorf *et al.* (2010) and
616 Kohn (2010) for modern leaf $\delta^{13}\text{C}$. Calculation of Cretaceous MAP from $\delta^{13}\text{C}_{\text{PLANT}}$

617 compilations using the proposed relationships is not possible. Information to compute the data
618 (plant functional type, altitude and latitude of growing site) is either missing or very vague,
619 and the plant substrate is mixed, i.e. derives from different plant tissues (amber, wood,
620 charcoal, coal, leaf, bulk terrestrial organic matter) for which the botanical affinity is largely
621 unknown.

622

623 Schubert and Jahren (2012) found a strong relationship between $\Delta^{13}\text{C}_\text{P}$ and $p\text{CO}_2$ for plants
624 grown in chambers with controlled environmental conditions. According to their model, plant
625 $\Delta^{13}\text{C}_\text{P}$ hyperbolically increases with increasing $p\text{CO}_2$ levels. This relationship was validated
626 against ice-core $p\text{CO}_2$ data for the Last Glacial Maximum and used to reconstruct the $p\text{CO}_2$ at
627 the Palaeocene–Eocene Thermal maximum (Schubert and Jahren, 2013, 2015). In contrast to
628 these studies, Cretaceous $\delta^{13}\text{C}_\text{AMBER}$ and $\delta^{13}\text{C}_\text{ISOORG}$ shows the most ^{13}C -enriched values in
629 intervals of predicted high $p\text{CO}_2$ and the most ^{13}C -depleted values in intervals of predicted
630 low $p\text{CO}_2$ (Fig. 7, see also Wang *et al.*, 2014), as also previously noted by Tappert *et al.*
631 (2013). Precise calculation of $\Delta^{13}\text{C}_\text{P}$ is not possible for our dataset, given the age uncertainties
632 of the samples and thus the difficulty in assigning to each $\delta^{13}\text{C}_\text{PLANT}$ data point a precise value
633 of $\delta^{13}\text{C}_\text{ATM}$. However, as previously described, comparison of the magnitude of the long-term
634 negative trend of $\delta^{13}\text{C}_\text{ATM}$ with the magnitude of amber and similar ISOORG $\delta^{13}\text{C}$ trend
635 suggests that $\Delta^{13}\text{C}_\text{P}$ increased in the Late Cretaceous. This result suggests that either $p\text{CO}_2$ has
636 no effect on plant $\delta^{13}\text{C}$ during the Cretaceous or that the $p\text{CO}_2$ reconstructions made via
637 biogeochemical modelling are incorrect. Similar to what was found in this study, Diefendorf
638 *et al.* (2015) found that $\Delta^{13}\text{C}_\text{P}$ does not increase in correspondence with intervals of high $p\text{CO}_2$
639 in the Palaeogene. Kohn (2016) found no or negligible $p\text{CO}_2$ dependence of $\delta^{13}\text{C}_\text{PLANT}$ in
640 selected Cenozoic case studies. This phenomenon is explained by the ability of plants to
641 evolve within decadal–centurial timescales in response to changing $p\text{CO}_2$ by adjusting their
642 physiology to maintain an ideal c_i/c_a ratio (Diefendorf *et al.*, 2015; Kohn *et al.*, 2016 and

643 references therein). By contrast, on shorter timescales (<1 year chamber growth experiments),
644 plants respond to changing $p\text{CO}_2$ through the stomata, thus changing the c_i/c_a (eq.1;
645 Diefendorf *et al.*, 2015).
646
647 The $\delta^{13}\text{C}$ of amber and plant tissues seems to decrease with increasing $p\text{O}_2$ levels, as
648 independently inferred by biogeochemical modelling (Berner 2009) and charcoal abundance
649 (Glasspool and Scott, 2010) (Fig. 7). Such a relationship is in line with theoretical
650 expectations and the results obtained in controlled chamber experiments, which show plant
651 $\Delta^{13}\text{C}$ increases by 1.5–3.5‰ in high (35%) $p\text{O}_2$ (Berner *et al.*, 2000; Beerling *et al.*, 2002). As
652 previously described, Tappert *et al.* (2013) proposed the use of $\delta^{13}\text{C}_{\text{AMBER}}$ to reconstruct
653 palaeo- $p\text{O}_2$, assuming that, at ambient air, the $\Delta^{13}\text{C}_p$ is proportional to $p\text{O}_2$ and that
654 physiological adaptations did not occur through time. The Cretaceous $p\text{O}_2$ model proposed by
655 Tappert *et al.* (2013) fails to reproduce the $p\text{O}_2$ trends calculated by other authors (Fig. 7) and
656 contradicts plant $\delta^{13}\text{C}$ data compiled in this study. This difference could be related to the
657 difficulty in calculating past $\delta^{13}\text{C}_{\text{ATM}}$ and the use of mean $\delta^{13}\text{C}_{\text{AMBER}}$, which are terms in the
658 equations proposed by Tappert *et al.* (2013) to infer $p\text{O}_2$ from $\delta^{13}\text{C}_{\text{AMBER}}$. Indeed, small
659 variations in growing conditions, such as light exposure, nutrient, and water levels, can mask
660 the $p\text{O}_2$ effect on plant $\delta^{13}\text{C}$, as shown during controlled chamber experiments (Beerling *et*
661 *al.*, 2002). Therefore, accurate reconstruction of past atmospheric $p\text{O}_2$ from mean $\delta^{13}\text{C}$ of
662 ambers is fraught with difficulties, given that the $\delta^{13}\text{C}$ of resin varies enormously, even at the
663 scale of a single tree (see section 3). Moreover, Tappert *et al.* (2013) assumed in their model
664 that physiological adaptations did not occur but, as discussed above, on long timescales plants
665 do evolve to maintain an ideal leaf–gas exchange optimum. The observed correspondence
666 between biogeochemical modelling and charcoal $p\text{O}_2$ records, and $\delta^{13}\text{C}_{\text{PLANT}}$ (both amber and
667 other tissues) points to a possible $p\text{O}_2$ effect on Cretaceous C3 $\Delta^{13}\text{C}_p$ that definitely deserves
668 further exploration.

669

670 **5. CONCLUSIONS**

671

672 Our carbon-isotope analysis of modern conifer resin and associated plant tissues showed that
673 Hardening after exudation causes an overall ^{13}C -enrichment in the bulk carbon-isotope
674 signature of resin. This is evident comparing the $\delta^{13}\text{C}$ of liquid-viscous (mean = -25.9‰) to
675 the $\delta^{13}\text{C}$ of solid resins (mean = -27.1‰) and is explained by selective loss of ^{13}C -depleted
676 volatiles. Carbon-isotope fractionation during resin biosynthesis occurs and results in a more
677 ^{13}C -enriched $\delta^{13}\text{C}_{\text{RESIN}}$ signature (by approx. $2\text{--}4\text{‰}$) than the $\delta^{13}\text{C}$ of other tissues sampled
678 from the same plant branch. By contrast, wood and leaf $\delta^{13}\text{C}$ show little difference ($<1\text{‰}$)
679 within the same branch. Results of this study suggest post-photosynthetic $\Delta^{13}\text{C}$ is larger in
680 resin than in other plant tissues. Furthermore, the variability of the $\delta^{13}\text{C}_{\text{RESIN}}$ is high (approx.
681 8‰), from -30.6‰ to -22.8‰ . $\delta^{13}\text{C}_{\text{RESIN}}$ shows differences of up to 6‰ between plant
682 species, locality and within a single tree. $\delta^{13}\text{C}_{\text{RESIN}}$ of different tree genera growing in the
683 same locality and at the same altitude shows differences of about $2\text{--}5\text{‰}$ $\delta^{13}\text{C}_{\text{RESIN}}$. $\delta^{13}\text{C}_{\text{RESIN}}$
684 seems to become more ^{13}C -enriched with increasing altitude. The environmental variability of
685 $\delta^{13}\text{C}$ of resin is similar to that reported for leaf and wood, suggesting the potential to record
686 changes in $\Delta^{13}\text{C}$ by C3 plants. Therefore, resin appears to be a valuable substrate for carbon-
687 isotope studies in modern plant ecology and physiology.

688

689 Our meta-analysis of new and published Cretaceous $\delta^{13}\text{C}_{\text{PLANT}}$ (amber, wood and mixed
690 substrates) revealed that Cretaceous $\delta^{13}\text{C}_{\text{AMBER}}$ (mean = $-22.3\text{‰} \pm 1.9\text{‰}$) is more ^{13}C -enriched
691 than other C3 plant material $\delta^{13}\text{C}$ (mean = $-24.2\text{‰} \pm 1.3\text{‰}$) and wood (mean = $-23.1\text{‰} \pm 1.3\text{‰}$),
692 as observed in modern plants. Therefore, fossil material can retain the same patterns observed
693 in modern samples, i.e. the differences being generated by $\Delta^{13}\text{C}$ during resin biosynthesis. In
694 the Cretaceous, $\delta^{13}\text{C}_{\text{AMBER}}$ has variability similar to modern resin, but the scatter of $\delta^{13}\text{C}_{\text{AMBER}}$

695 data is larger than the scatter of $\delta^{13}\text{C}$ data of other fossil C3 plant material, which is attributed
696 to diagenesis. Amber has been shown to become a closed system with respect to carbon
697 isotopes soon after hardening, whereas other plant remains can experience a more pervasive
698 diagenetic overprint (both ^{13}C enrichment or depletion). Diagenetic processes could be
699 responsible also for narrowing $\delta^{13}\text{C}$ variability by selectively removing specific compounds.
700 These observations suggest amber can preserve the pristine $\delta^{13}\text{C}$ signature better than other
701 plant tissues and, consequently, the original high $\delta^{13}\text{C}$ variability as shown by modern plants.
702 Thus, amber can retain faithful information about past environments and climate.
703 Despite the large variability, amber, wood, and mixed plant (ISOORG) record similar long-
704 term trends during the Cretaceous. In particular, plant material record a 2.5–3‰ negative
705 trend from the Hauterivian–Barremian to the Maastrichtian that mirrors a similar but smaller
706 (1‰) shift in the $\delta^{13}\text{C}$ of the atmosphere calculated from benthic foraminifera $\delta^{13}\text{C}$ and $\delta^{18}\text{O}$
707 data compilation. Increasing mean annual precipitation and/or $p\text{O}_2$ levels could have
708 increased $\Delta^{13}\text{C}$ of plants during the Cretaceous, thus increasing the magnitude of the negative
709 trend. Comparing the isotopic records with $p\text{CO}_2$ trends suggests that $p\text{CO}_2$ did not affect
710 plant $\Delta^{13}\text{C}$ on the long-time scales considered in this study.

711

712 Our study thus shows that in the deep past the interpretation of the $\delta^{13}\text{C}_{\text{AMBER}}$ curve and, by
713 extension, the $\delta^{13}\text{C}$ of terrestrial plants, is ambiguous to some extent due to the difficulty in
714 constraining the environmental and physiological factors that control the natural variability of
715 $\delta^{13}\text{C}_{\text{RESIN}}$ and the uncertainties in determining the age of some of the analysed material.
716 However, meta-analysis of marine and terrestrial $\delta^{13}\text{C}$ records coupled to the amber record
717 reveals isotopic variations that seem ascribable to changes in the composition of the
718 Cretaceous atmosphere–ocean system and climate. Improvement of the resolution of the
719 existing data and collection of information about botanical source and environmental growing

720 conditions of the fossil plant material will undoubtedly improve our understanding of amber
721 $\delta^{13}\text{C}$ records and allow more faithful reconstruction of the past atmosphere.

722

723 **ACKNOWLEDGEMENTS**

724

725 We thank V. Perrichot (Rennes, France) and A. Wolfe (Edmonton, Canada) for providing
726 amber samples for this study, and the Botanical Garden of Padova University (Italy) for
727 permission to collect samples of resins. Fieldwork and collection in southern New Caledonia
728 were kindly permitted by the Direction de l'Environnement (Province Sud) permit n°
729 17778/DENV/SCB. We are indebted to P. Ditchfield for isotope analyses of amber at the
730 Research Laboratory for Archaeology and the History of Art (Oxford, UK). C. Agnini and M.
731 Rigo (Padova, Italy) contributed to the fine-tuning of IRMS methods at the University of
732 Padova. D. L. Dilcher (Bloomington, USA), K. Schmidt (Jena, Germany) and J. Munzinger
733 (Nouméa, New Caledonia) kindly supported the fieldwork in the USA and in New Caledonia.
734 We thank C.E. Reymond (ZMT Bremen, Germany) for suggestions during the revision of the
735 manuscript. We thank D.R. Gröcke, two anonymous reviewers and the editor A.L. Sessions
736 for the useful comments and suggestions that greatly improved the manuscript.

737

738 **FUNDING**

739

740 This work was supported by a “Young Researcher Grant” from the University of Padova, Italy
741 (P.I. Jacopo Dal Corso; grant number: DALCPRGR12), by the Spanish Ministry of Economy
742 and Competitiveness (project “AMBERIA”; grant number: CGL2014-52163), and by the
743 German Research Foundation, project number SE 2335/3-1. LJS is supported by DFG project
744 SE 2335/3-1 at the University of Göttingen, Germany. J. Dal Corso is currently supported by
745 a junior research fellowship at the Hanse-Wissenschaftskolleg (Delmenhorst, Germany).

746

747 **REFERENCES**

748

- 749 Aquilina L., Girard V., Henin O., Bouhnik-Le Coz M., Vilbert D., Perrichot V., Néraudeau D.
750 (2013) Amber inorganic geochemistry: New insights into the environmental processes in a
751 Cretaceous forest of France. *Palaeogeography, Palaeoclimatology, Palaeoecology*, **369**,
752 220–227.
- 753 Arens N.C., Jahren A.H., Amundson R. (2000) Can C₃ plants faithfully record the carbon
754 isotopic composition of atmospheric dioxide? *Paleobiology*, **26**, 137–164.
- 755 Badeck F.W., Tcherkez G., Nogues S., Piel C., Ghashghaie J. (2005) Post-photosynthetic
756 fractionation of stable carbon isotopes between plant organs - a widespread phenomenon.
757 *Rapid Communications in Mass Spectrometry*, **19**, 1381–1391.
- 758 Barrón E., Peyrot D., Rodríguez-López J.P., Meléndez N., López-del Valle R., Najarro M.,
759 Rosales I., Comas-Rengifo M.J. (2015) Palynology of Aptian and upper Albian (Lower
760 Cretaceous) amber-bearing outcrops of the southern margin of the Basque-Cantabrian
761 basin (northern Spain). *Cretaceous Research*, **52**, 292–312.
- 762 Batten D., Colin J.P., Néraudeau D. (2010) Megaspores from mid Cretaceous deposits in
763 western France and their biostratigraphic and palaeoenvironmental significance. *Review of*
764 *Palaeobotany and Palynology*, **161**, 151–167.
- 765 Bechtel A., Sachsenhofer R.F., Gratzner R., Lucke A., Puttmann W. (2002) Parameters
766 determining the carbon isotopic composition of coal and wood in the Early Miocene
767 Oberdorf lignite seam (Styrian Basin, Austria). *Organic Geochemistry*, **33**, 1001–1024.
- 768 Bechtel A., Gratzner R., Sachsenhofer R.F., Gusterhuber J., Lucke A., Puttmann W. (2008)
769 Biomarker and carbon isotope variation in coal and fossil wood of Central Europe through
770 the Cenozoic. *Palaeogeography, Palaeoclimatology, Palaeoecology*, **226**, 166–175.

- 771 Beerling D.J., Lake J.A., Berner R.A., Hickley L.J., Taylor D.W., Royer D.L. (2002) Carbon
772 isotope evidence implying high O₂/CO₂ ratios in the Permo-Carboniferous atmosphere.
773 *Geochimica et Cosmochimica Acta*, **66**, 3757–3767.
- 774 Berner R.A. (1994) GEOCARB II: A revised model of atmospheric CO₂ over Phanerozoic
775 time. *American Journal of Science*, **294**, 56–91.
- 776 Berner R.A. (2001) Modelling atmospheric O₂ over Phanerozoic time. *Geochimica et*
777 *Cosmochimica Acta*, **65**, 685–94.
- 778 Berner R.A. (2006) Inclusion of the weathering of volcanic rocks in the GEOCARBSULF
779 model. *American Journal of Science*, **306**, 295–302.
- 780 Berner R.A. (2009) Phanerozoic atmospheric oxygen: New results using the
781 GEOCARBSULF model. *American Journal of Science*, **309**, 603–606.
- 782 Berner R.A., Petsch S.T., Lake J.A., Beerling D.J., Popp B.N., Lane R.S., Laws E.A., Westley
783 M.B., Cassar N., Woodward F.I., Quick W.P. (2000) Isotope fractionation and atmospheric
784 oxygen: Implications for Phanerozoic O₂ evolution. *Science*, **287**, 1630–1633.
- 785 Bodin S., Meissner P., Janssen N.M.M., Steuber T., Mutterlose J (2015) Large igneous
786 provinces and organic carbon burial: Controls on global temperature and continental
787 weathering during the Early Cretaceous. *Global and Planetary Change*, **133**, 238–253.
- 788 Bonal D., Sabatier D., Montpied P., Tremeaux D, Guehl J.M. (2000) Interspecific variability
789 of δ¹³C among trees in rainforest of French Guiana: functional groups and canopy
790 integration. *Oecologia*, **124**, 454–468.
- 791 Cerling T.E., Harris J.M. (1999) Carbon isotope fractionation between diet and bioapatite in
792 ungulate mammals and implications for ecological and paleoecological studies.
793 *Oecologia*, **120**, 347–363.
- 794 Cernusak L.A., Tcherkez G., Keitel C., Cornwell W.K., Santiago L.S., Knoch A., Barbour
795 M.M., Williams D.G., Reich P.B., Ellsworth D.S., Dawson T.E., Griffiths H.G., Farquhar
796 G.D., Wright I.J. (2009) Why are non-photosynthetic tissues generally ¹³C enriched

- 797 compared with leaves in C₃ plants? Review and synthesis of current hypotheses.
798 *Functional Plant Biology*, **36**, 199–213.
- 799 Cernusak L.A., Ubierna N., Winter K., Holtum J.A.M., Marshall J.D., Farquhar G.D. (2013)
800 Environmental and physiological determinants of carbon isotope discrimination in
801 terrestrial plants. *New Phytologist*, **200**, 950–965.
- 802 Coplen T.B., Brand W.A., Gehre M., Gröning M., Meijer H.A.J., Toman B., Verkouteren R.M.
803 (2006) New Guidelines for ¹³C Measurements. *Analytical Chemistry*, **78** (7), 2439–2441.
- 804 Dal Corso J., Preto N., Kustatscher E., Mietto P., Roghi G., Jenkyns H. (2011). Carbon-
805 isotope variability of Triassic amber, as compared with wood and leaves (Southern Alps,
806 Italy). *Palaeogeography, Palaeoclimatology, Palaeoecology*, **302**, 187–193.
- 807 Dal Corso J., Roghi G., Ragazzi E., Angelini I., Giarretta A., Soriano C., Delclòs X., Jenkyns
808 H.C. (2013) Physico-chemical analysis of Albian (Lower Cretaceous) amber from San
809 Just (Spain): implications for palaeoenvironmental and palaeoecological studies.
810 *Geologica Acta*, **11**, 359–370.
- 811 Diefendorf A.F., Mueller K.E., Wing S.L., Koch P.L., Freeman K.H. (2010) Global patterns in
812 leaf ¹³C discrimination and implications for the studies of past and future climate.
813 *Proceeding of the National Academy of Science*, **107**, 5738–5743.
- 814 Diefendorf A.F., Freeman K.H., Wing S.L. (2012) Distribution and carbon isotope patterns of
815 diterpenoids and triterpenoids in modern temperate C₃ trees and their geochemical
816 significance. *Geochimica et Cosmochimica Acta*, **85**, 342–356.
- 817 Diefendorf A.F., Freeman K.H., Wing S.L., Curran E.D., Mueller K.E. (2015) Paleogene
818 plants fractionated carbon isotope similar to modern plants. *Earth and Planetary Science
819 Letters*, **429**, 33–44.
- 820 Duursma R.A., Marshall J.D. (2006) Vertical canopy gradients in δ¹³C correspond with leaf
821 nitrogen content in a mixed-species conifer forest. *Trees*, **20**, 496–506.

- 822 Erba E (2004) Calcareous nannofossils and Mesozoic oceanic anoxic events. *Marine*
823 *micropaleontology*, **52**, 85–106.
- 824 Farquhar G.D., Ehleringer J.R., Hubick K.T. (1989) Carbon isotope discrimination and
825 photosynthesis. *Annual Review of Plant Physiology and Plant Molecular Biology*, **40**,
826 503–538.
- 827 Friedrich O., Norris R.D., Erbacher J. (2012) Evolution of middle to Late Cretaceous oceans—
828 A 55 m.y. record of Earth’s temperature and carbon cycle. *Geology*, **40(2)**, 107–110.
- 829 Gasulla J.M., Ortega F., Pereda-Suberbiola X., Escaso F., Sanz J.L. (2011) Elementos de la
830 armadura dérmica del dinosaurio anquilosaurio *Polacanthus* Owen, 1865, en el Cretácico
831 Inferior de Morella (Castellón, España). *Ameghiniana*, **48**, 508–519
- 832 Girard V., Schmidt A.R., Saint-Martin S., Struwe S., Perrichot V., Saint-Martin J.P., Breton G.,
833 Néraudeau D. (2008) Exceptional preservation of marine diatoms in upper Albian amber.
834 *Proceeding of the National Academy of Science*, **105**, 17426–17429.
- 835 Glasspool I.J., Scott A.C (2010) Phanerozoic concentrations of atmospheric oxygen
836 reconstructed from sedimentary charcoal. *Nature Geoscience*, **3**, 627–630.
- 837 Gomez B., Barale G., Saad D., Perrichot V. (2003) Santonian Angiosperm-dominated leaf-
838 assemblage from Piolenc (Vaucluse, Sud-Est de la France). *C.R. Palevol*, **2(3)**, 197–204.
- 839 Gradstein F.M., Ogg J.G., Schmitz M., Ogg G. (2012) *The Geologic Time Scale 2012 2-*
840 *Volume Set, 1st Edition*. Elsevier.
- 841 Gröcke D.R. (1998) Carbon-isotope analyses of fossil plants as a chemostratigraphic and
842 palaeoenvironmental tool. *Lethaia*, **31**, 1–13.
- 843 Gröcke D.R. (2002) The carbon isotope composition of ancient CO₂ based on higher-plant
844 organic matter. *Philosophical Transaction of the Royal Society A*, **360**, 633–658.
- 845 Gröcke, D.R., Hesselbo, S.P., Jenkyns, H.C., 1999. Carbon-isotope composition of Lower
846 Cretaceous fossil wood: Ocean-atmosphere chemistry and relation to sea-level change.
847 *Geology*, **27**, 155–158.

- 848 Hall G., Woodborne S., Scholes M. (2008) Stable carbon isotope ratios from archeological
849 charcoals as palaeoenvironmental indicators. *Chemical Geology*, **247**, 384–400
- 850 Hesselbo S.P., Jenkyns H.C., Duarte L.V., Oliveira L.C. (2007) Carbon-isotope record of the
851 Early Jurassic (Toarcian) Oceanic Anoxic Event from fossil wood and marine carbonate
852 (Lusitanian Basin, Portugal). *Earth and Planetary Science Letters*, **253**, 455–470.
- 853 Hudson J.D., Anderson T.F. (1989) Ocean temperatures and isotopic composition through
854 time. *Transactions of the Royal Society of Edinburgh*, **80**, 183–192.
- 855 Hultine K.R., Marshall J.D. (2000) Altitude trends in conifer leaf morphology and stable
856 carbon isotope composition. *Oecologia*, **123**, 32–40.
- 857 Jahren A.H., Arens N.C., Harbeson S.A. (2008) Prediction of atmospheric $\delta^{13}\text{C}\text{O}_2$ using fossil
858 plant tissues. *Review of Geophysics*, **46**, RG1002, doi:10.1029/2006RG000219.
- 859 Jones T.P., Chaloner W.G. (1991) Fossil charcoal, its recognition and palaeoatmospheric
860 significance. *Palaeogeography, Palaeoclimatology, Palaeoecology*, **97**, 39–50.
- 861 Kohn M.J. (2010) Carbon isotope compositions of terrestrial C3 plants as indicators of
862 (paleo)ecology and (paleo)climate. *Proceeding of the National Academy of Science*, **107**,
863 19691–19695.
- 864 Kohn M.J. (2016) Carbon isotope discrimination in C3 land plants is independent of natural
865 variations in pCO₂. *Geochemical Perspectives Letters*, **2**, 35–43.
- 866 Körner C., Farquhar G.D., Roksandic Z. (1988) A global survey of carbon isotope
867 discrimination in plants from high altitude. *Oecologia*, **74**, 623–632.
- 868 Körner C., Farquhar G.D., Wong S.C. (1991) Carbon isotope discrimination by plants follows
869 latitudinal and altitudinal trends. *Oecologia*, **88**, 30–40.
- 870 Krzywinski M., Altman N. (2014) Visualizing samples with box plots. *Nature Methods*, **11**,
871 119–120.

- 872 Lambert J.B., Santiago-Blay J.A., Anderson K.B. (2008) Chemical signatures of fossilized
873 resins and recent plant exudates. *Angewandte Chemie International Edition*, **47**, 9608–
874 9616.
- 875 Langenheim J.H. (1990) Plant resins. *American Scientist*, **78**, 16–24.
- 876 Leavitt S.W., Long A. (1986) Stable-carbon isotope variability in tree foliage and wood.
877 *Ecology*, 67(4), 1002–1010.
- 878 Li X., Jenkyns H.C., Zhang C., Wang Y., Liu L., Cao K. (2013) Carbon isotope signatures of
879 pedogenic carbonates from SE China: rapid atmospheric $p\text{CO}_2$ changes during the middle-
880 late Early Cretaceous time. *Geological Magazine*, **115**, 830–849.
- 881 López-Horgue M.A., Owen H.G., Rodríguez-Lázaro J., Orue-Etxebarria U., Fernández-
882 Mendiola P.A., García-Mondéjar J. (1999) Late Albian–Early Cenomanian stratigraphic
883 succession near Estella-Lizarra (Navarra, central northern Spain) and its regional and
884 interregional correlation. *Cretaceous Research*, **20**, 369–402.
- 885 Maksoud S., Granier B., Azar D., Gèze R., Paicheler J.-C., Bedmar J.A.M. (2014) Revision of
886 “Falaise de Blanche” (Lower Cretaceous) in Lebanon, with definition of a Jezzin regional
887 Stage. *Carnets de Géologie*, **14**, 401–427.
- 888 Maksoud S., Azar D., Granier B., Gèze R. (in press) New data on the age of the Lower
889 Cretaceous amber outcrops of Lebanon. *Palaeoworld*,
890 <http://dx.doi.org/10.1016/j.palwor.2016.03.003>
- 891 McKellar R.C., Wolfe A.P., Tappert R., Muehlenbachs K. (2008) Correlation of Grassy Lake
892 and Cedar Lake ambers using infrared spectroscopy, stable isotopes, and
893 palaeontomology. *Canadian Journal of Earth Sciences*, **45**, 1061–1082.
- 894 McKellar R.C., Wolfe A.P., Muehlenbachs K., Tappert R., Engel M.S., Cheng T., Sanchez-
895 Azofeifa A. (2011) Insect outbreaks produce distinctive carbon isotope signatures in
896 defensive resins and fossiliferous ambers. *Proceedings of the Royal Society B*, DOI:
897 10.1098/rspb.2011.0276.

- 898 Menor-Salván C., Najjarro M., Velasco F., Rosales I., Tornos F., Simoneit B.R.T. (2010)
899 Terpenoids in extracts of Lower Cretaceous ambers from the Basque-Cantabrian Basin (El
900 Soplaio, Cantabria, Spain): Paleochemotaxonomic aspects. *Organic Geochemistry* **41**,
901 1089–1103.
- 902 Murray A.P., Padley D., McKirdy D.M., Booth W.E., Summons R.E. (1994) Oceanic transport
903 of fossil dammar resin: The chemistry of coastal resinites from South Australia.
904 *Geochimica et Cosmochimica Acta*, **58**, 3049–3059.
- 905 Murray A.P., Edwards D., Hope J.M., Boreham C.J., Booth W.E., Alexander R.A., Summons
906 R.E. (1998) Carbon isotope biogeochemistry of plant resins and derived hydrocarbons.
907 *Organic Geochemistry*, **29**, 1199–1214.
- 908 Néraudeau D., Vullo R., Gomez B., Girard V., Lak M., Videt B., Dépré E., Perrichot V. (2009)
909 Amber, plant and vertebrate fossils from the Lower Cenomanian paralic facies of Aix
910 Island (Charente-Maritime, SW France). *Geodiversitas*, **31(1)**, 13–27.
- 911 Nissenbaum A., Yakir D. (1995) Stable isotope composition of amber. In: *Amber, resinite, and*
912 *fossil resins* (eds. Anderson K.B. and Crelling J.C.). ACS Symposium series, American
913 Chemical Society, Washington, pp. 32–42.
- 914 Nohra Y.A., Perrichot V., Jeanneau L., Le Pollès L., Azar D. (2015). Chemical
915 characterization and botanical origin of French ambers. *Journal of Natural Products*,
916 **78(6)**, 1284–1293.
- 917 Nordt L., Tubbs J., Dworkin S. (2016) Stable carbon isotope record of terrestrial organic
918 materials for the last 450 Ma yr. *Earth-Science Reviews*, **159**, 103–117.
- 919 Peñalver E., Delclòs X. (2010) Spanish amber, in: Penney, D. (Ed.), *Biodiversity of fossils in*
920 *amber from the major world deposits*. Siri Scientific Press, Manchester, pp. 236–271.
- 921 Peyrot D., Jolly D., Barron E. (2005) Apport de données palynologiques à la reconstruction
922 paléoenvironnementale de l'Albo-Cénomaniien des Charentes (Sud-Ouest de la France).
923 *C.R. Palevol*, **4**, 151–165.

- 924 Prokoph A., Shields G.A., Veizer J. (2008) Compilation and time-series analysis of marine
925 carbonate $\delta^{18}\text{O}$, $\delta^{13}\text{C}$, $^{87}\text{Sr}/^{86}\text{Sr}$ and $\delta^{34}\text{S}$ database through Earth history. *Earth-Science*
926 *Reviews*, **87**, 113–133.
- 927 Pujalte V., Robles S. (2008) Parasecuencias transgresivo-regresivas en un cortejo
928 transgresivo: parte superior de la Fm Utrillas en Olleros de Pisuerga, Palencia. *Geogaceta*,
929 **44**, 187–190.
- 930 Ragazzi E., Schmidt A.R. (2011) Amber, in: Reitner, J., and Thiel, V. (Eds.), *Encyclopedia of*
931 *Geobiology*. Springer, The Netherlands, pp. 24–36.
- 932 Ragazzi E., Giaretta A., Perrichot V., Néraudeau D., Schmidt A.R., Roghi G. (2009) Thermal
933 analysis of Cretaceous ambers from Southern France. *Geodiversitas*, **31(1)**, 163–175.
- 934 Rodríguez-López J.P., Meléndez N., Soria A.R., de Boer P.L. (2009) Reinterpretación
935 estratigráfica y sedimentológica de las formaciones Escucha y Utrillas de la Cordillera
936 Ibérica. *Revista de la Sociedad Geológica de España*, **22**, 163–219.
- 937 Saint Martin S., Saint Martin J.P., Girard V., Néraudeau D. (2013) Organismes filamenteux de
938 l'ambre du Santonien de Belcodène (Bouches-du-Rhône, France). *Annales de*
939 *Paléontologie*, **99(4)**, 339–359.
- 940 Scalarone D., van der Horst J., Boon J.J., Chiantore O. (2003) Direct-temperature mass
941 spectrometric detection of volatile terpenoids and natural terpenoid polymers in fresh and
942 artificially aged resins. *Journal of Mass Spectrometry*, **38**, 607–617.
- 943 Scotese C.R. (2002) <http://www.scotese.com>, (PALEOMAP website).
- 944 Schubert B.A., Jahren A.H. (2012) The effect of atmospheric CO₂ concentration on carbon
945 isotope fractionation in C₃ land plants. *Geochimica et Cosmochimica Acta*, **96**, 29–43.
- 946 Schubert B.A., Jahren A.H. (2013) Reconciliation of marine and terrestrial carbon isotope
947 excursions based on changing atmospheric CO₂ levels. *Nature Communications*, **4:1653**.

- 948 Schubert B.A., Jahren A.H. (2013) Global increase in carbon isotope fractionation following
949 the Last Glacial Maximum caused by increase in atmospheric $p\text{CO}_2$. *Geology*, **43**, 435–
950 438.
- 951 Cui Y., Schubert B.A. (2016) Quantifying uncertainty of past $p\text{CO}_2$ determined from changes
952 in C3 plant carbon isotope fractionation. *Geochimica et Cosmochimica Acta*, **172**, 127–
953 138.
- 954 Salazar-Jaramillo S., Fowell S.J., McCarthy P.J., Benowitz J.A., Sliwinski M.G., Tomisich
955 C.S. (2016) Terrestrial isotopic evidence for a Middle-Maastrichtian warming event from
956 the lower Cantwell Formation, Alaska. *Palaeogeography, Palaeoclimatology,*
957 *Palaeoecology*, **441**, 360–376.
- 958 Spiker E.C., Hatcher P.G. (1987) The effects of early diagenesis on the chemical and stable
959 carbon isotopic composition of wood. *Geochimica et Cosmochimica Acta*, **51**, 1385–1391.
- 960 Stern B., Lampert Moore C.D., Heron C., Pollard A.M. (2008) Bulk stable light isotopic ratios
961 in recent and archaeological resins: towards detecting the transport of resins in antiquity?
962 *Archaeometry*, **50**, 351-370.
- 963 Strauss H., Peters-Kottig W. (2003) The Paleozoic to Mesozoic carbon cycle revisited: The
964 carbon isotopic composition of terrestrial organic matter. *Geochemistry, Geophysics,*
965 *Geosystems*, **4(10)**, 1083.
- 966 Tappert R., McKellar R., Wolfe A.P., Tappert M.C., Ortega-Blanco J., Muehlenbachs K.
967 (2013) Stable carbon isotopes of C3 plant resins and ambers record changes in
968 atmospheric oxygen since the Triassic. *Geochimica et Cosmochimica Acta*, **121**, 240–262.
- 969 Thomas B.R. (1969) Kauri resins – Modern and Fossils. In: *Organic Geochemistry* (eds.
970 Eglinton E, Murphy MTJ). Springer Berlin Heidelberg, pp. 599–618.
- 971 Tipple B.J., Pagani M. (2007) The early origins of terrestrial C4 photosynthesis. *Annual*
972 *Review of Earth and Planetary Sciences*, **35**, 435–461.

- 973 Tipple B.J., Meyers S.R., Pagani M. (2010) Carbon isotope ratio of Cenozoic CO₂: A
974 comparative evaluation of available geochemical proxies. *Paleoceanography*, **25**, PA3202.
- 975 van Bergen P.F., Poole I. (2002) Stable carbon isotopes of wood: a clue to palaeoclimate?
976 *Palaeogeography, Palaeoclimatology, Palaeoecology*, **182**, 31-45.
- 977 Villanueva-Amadoz U., Pons D., Diez J.B., Ferrer J., Sender L.M. (2010) Angioperm pollen
978 grains of San just (Escucha Formation) from the Albian of the Iberian Range (north-
979 eastern Spain). *Review of Palaeobotany and Palynology*, **162**, 362–381.
- 980 Wallmann K. (2001) Controls on the Cretaceous and Ceno- zoic evolution of seawater
981 composition, atmospheric CO₂ and climate. *Geochimica et Cosmochimica Acta*, **18**, 3005–
982 3025.
- 983 Wang Y., Huang C., Sun B., Quan C., Wu J., Lin Z. (2014) Paleo-CO₂ variation trends and the
984 Cretaceous greenhouse climate. *Earth-Science Reviews*, **129**, 136–147.
- 985 Warren C.R., McGrath J.F., Adams M.A. (2001) Water availability and carbon isotope
986 discrimination in conifers. *Oecologia*, **127**, 476–486.
- 987 Yans J., Gerards T., Gerrienne P., Spagna P., Dejax J., Schnyder J., Storme J.-Y., Keppens E.
988 (2010) Carbon-isotope analysis of fossil wood and dispersed organic matter from the
989 terrestrial Wealden facies of Hautrage (Mons Basin, Belgium). *Palaeogeography,*
990 *Palaeoclimatology, Palaeoecology*, 291, 85–105.
- 991 Zhang J.W., Cregg B.M. (1996) Variation in stable isotope discrimination among and within
992 exotic conifer species grown in eastern Nebraska, USA. *Forest Ecology and Management*,
993 **83**, 181–187.

994

995 **FIGURE CAPTIONS**

996

997 **Figure 1.** Location of the sampling sites of modern resins (A) and Cretaceous amber (B)
998 analysed for carbon isotopes. Red dots = this study; orange dots = previous studies
999 (Nissenbaum & Yakir, 1995; Dal Corso *et al.*, 2013; Tappert *et al.*, 2013).

1000

1001 **Figure 2.** Distribution of modern resin $\delta^{13}\text{C}$ (orange histogram) and range of variability of
1002 modern C3 plants from Cerling & Harris (1999) and Tipple & Pagani (2007).

1003

1004 **Figure 3.** A) Carbon-isotope composition of liquid–viscous vs solid modern resin (Students' *t*-
1005 test *p* value = 0.001). Resin data are compared to a compilation of leaf data taken from
1006 Diefendorf *et al.* (2010). Data are represented as box-and-whiskers plots in order to highlight
1007 differences in distribution. The bars represent the first and fourth quartile, the box represents
1008 the second and third quartile, and the mid-line is the median. All investigated species of both
1009 genera are considered. Variation of the carbon-isotope composition (B) of solid resin, wood
1010 and leaves from different trees (two trees of *Araucaria heterophylla*, a *Picea abies* tree and a
1011 *Cupressus arizonica* tree) and (C) of solid resin collected from a single tree of *Araucaria*
1012 *heterophylla* at different heights. Samples in boxes (B) and (C) were collected in the botanical
1013 gardens of the University of Padova.

1014

1015 **Figure 4.** Carbon-isotope data of (A) modern liquid–viscous resin, and (B) *Pinus* and
1016 *Araucaria* resin plotted against altitude of the plant-growing site.

1017

1018 **Figure 5.** (A) Comparison of the $\delta^{13}\text{C}$ data distribution of Cretaceous C3 plant material from
1019 the ISOORG database (Nordt *et al.*, 2016) with amber. (B) Box-and-whiskers plots of $\delta^{13}\text{C}$
1020 data of modern leaves (Diefendorf *et al.*, 2010) and resin (this study), and Cretaceous
1021 ISOORG plants (Nordt *et al.*, 2016), wood (Nordt *et al.*, 2016; Salazar-Jaramillo *et al.*, 2016)

1022 and amber (this study; Nissenbaum & Yakir, 1995; Dal Corso *et al.*, 2013; Tappert *et al.*,
1023 2013).

1024

1025 **Figure 6.** Carbon-isotope ($\delta^{13}\text{C}$) curves from Cretaceous amber, terrestrial organic matter,
1026 marine carbonate. $\delta^{13}\text{C}$ data from plant material was grouped in 5Myrs bins following the
1027 method used by Nordt *et al.* (2016) and a third-degree polynomial curve was fit to the plant
1028 data to highlight the main trends shown through the Cretaceous (see text for further
1029 explanation). (A) Compilation of Cretaceous amber carbon-isotope data from this study and
1030 Nissenbaum & Yakir (1995), Dal Corso *et al.* (2013) and Tappert *et al.* (2013). (B) Wood $\delta^{13}\text{C}$
1031 data from Nordt *et al.* (2016) and Salazar-Jaramillo *et al.* (2016). (C) ISOORG $\delta^{13}\text{C}$ data from
1032 Nordt *et al.* (2016). ISOORG database comprises isotopic data from wood, leaf, charcoal,
1033 coal, palaeosols, bulk terrestrial organic matter. (D) Marine carbonate carbon-isotope data
1034 from planktonic and benthic foraminifera, and belemnites (Prokoph *et al.*, 2008 and Bodin *et*
1035 *al.*, 2015). Whole-rock general carbonate curve (black line) replotted from Erba (2004). The
1036 arrows represent the main carbonate $\delta^{13}\text{C}$ trend during the Cretaceous. Time scale after
1037 Gradstein *et al.* (2012).

1038

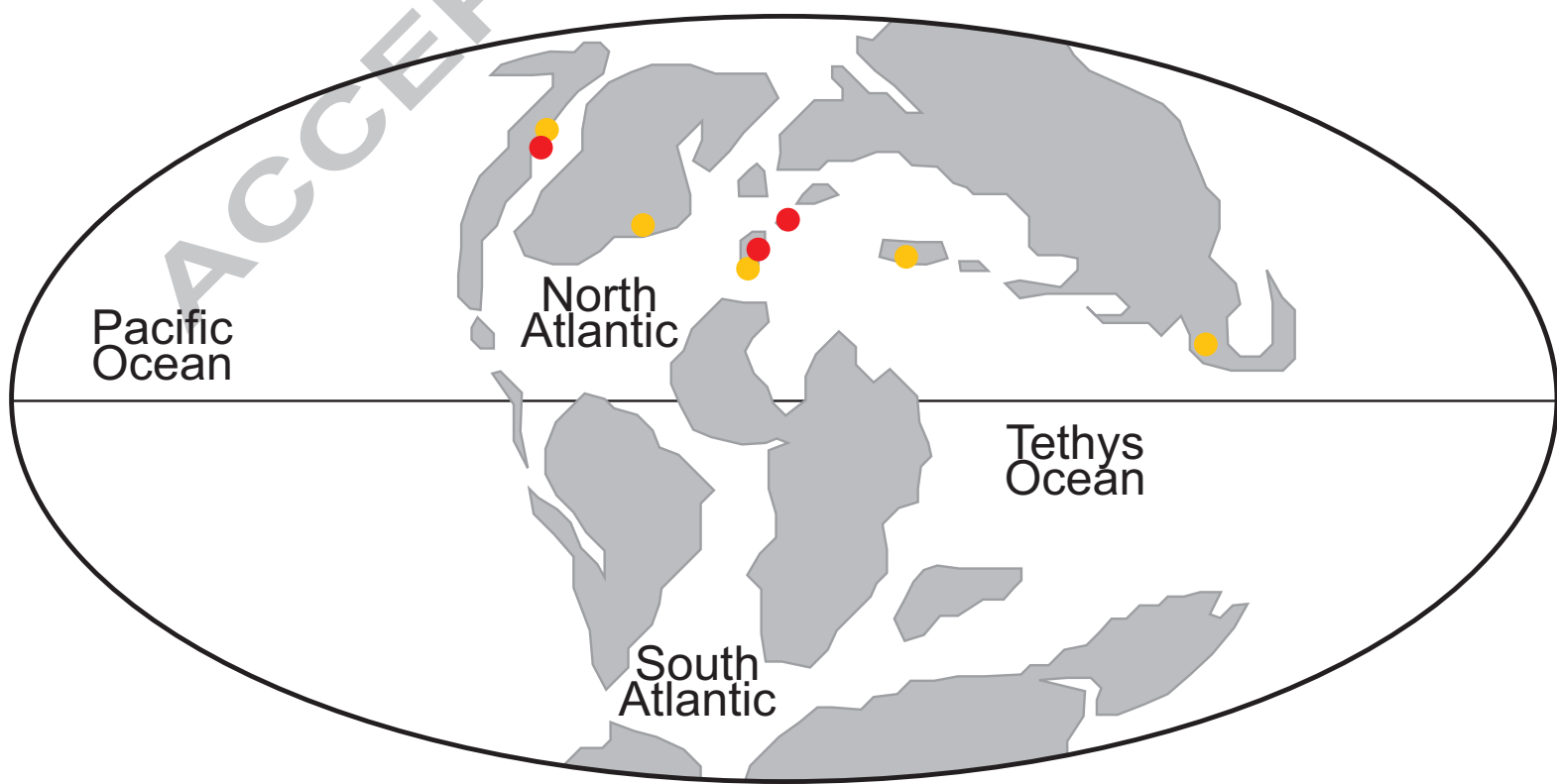
1039 **Figure 7.** Plant (amber and other tissues from the ISOORG database) $\delta^{13}\text{C}$ trends during the
1040 Cretaceous compared with the carbon-isotope composition of the atmosphere ($\delta^{13}\text{C}_{\text{ATM}}$)
1041 calculated from benthic foraminifera $\delta^{13}\text{C}$ and $\delta^{18}\text{O}$ (from Prokoph *et al.*, 2008), the Mean
1042 Annual Precipitation (MAP) as reconstructed from compact-corrected depth to calcic horizon
1043 in palaeosols in the Colorado Plateau (Retallack, 2009), the $p\text{CO}_2$ calculated by different
1044 biogeochemical models, and the $p\text{O}_2$ inferred from charcoal abundance (Glasspool and Scott,
1045 2010), biogeochemical modelling (Berner, 2009), and amber $\delta^{13}\text{C}$ (Tappert *et al.*, 2013).

1046

Modern Resins



Cretaceous (Albian - Cenomanian) resins



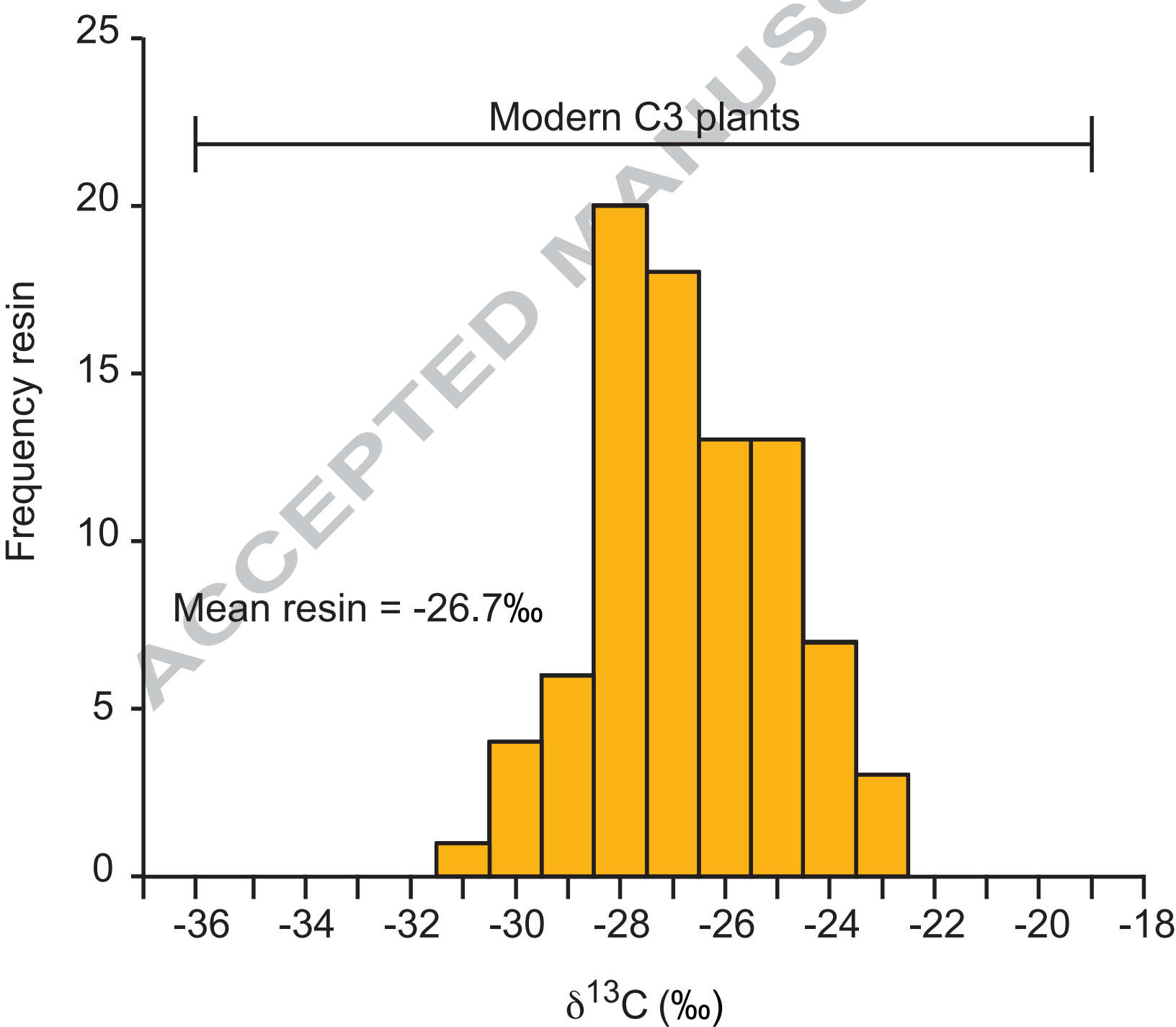
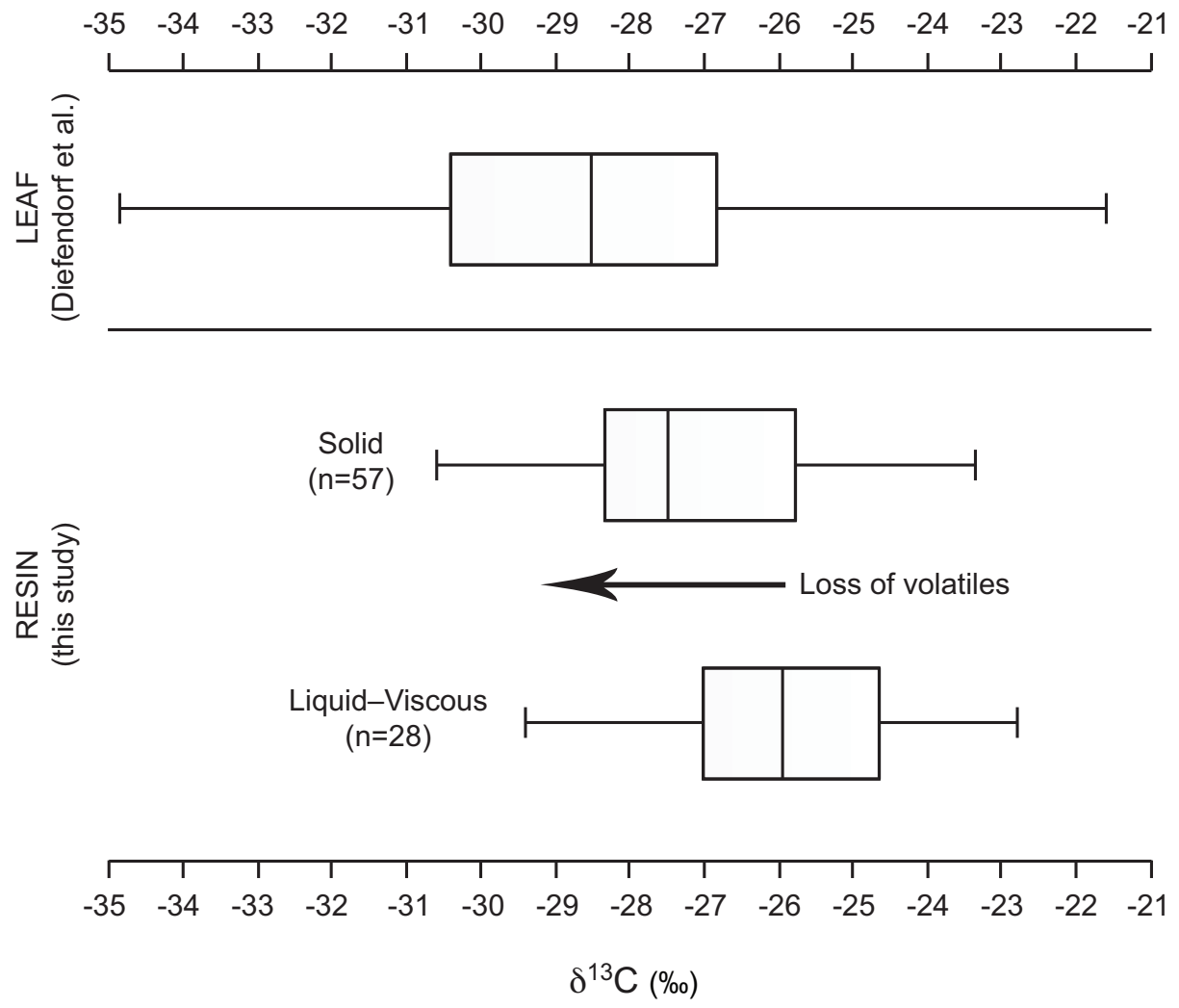
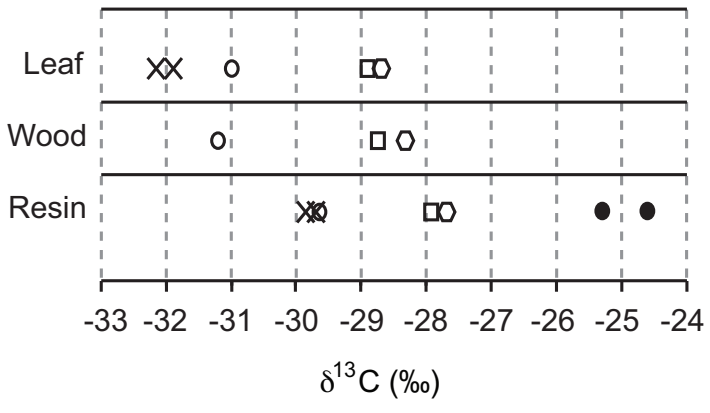


Figure 3

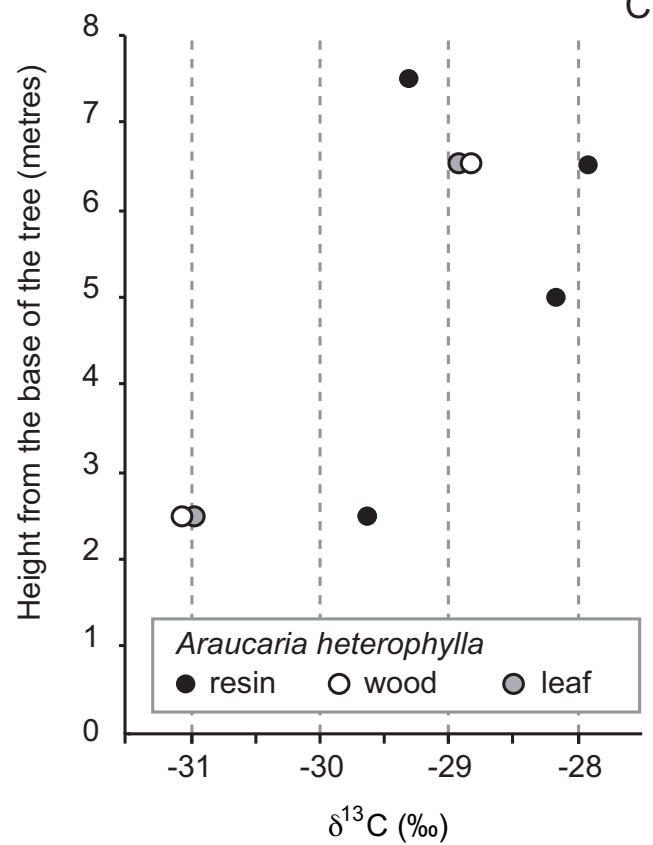
A



B



C



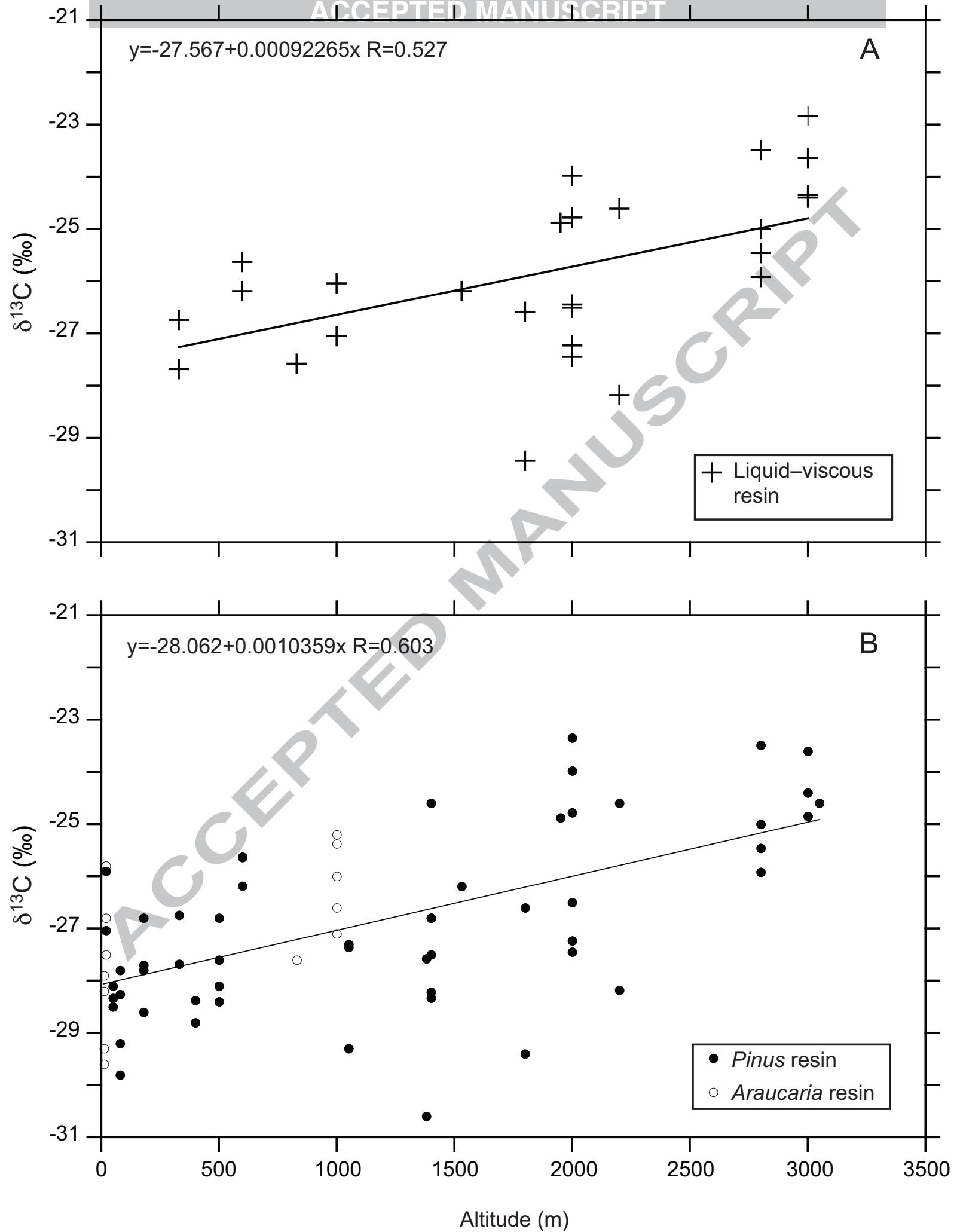


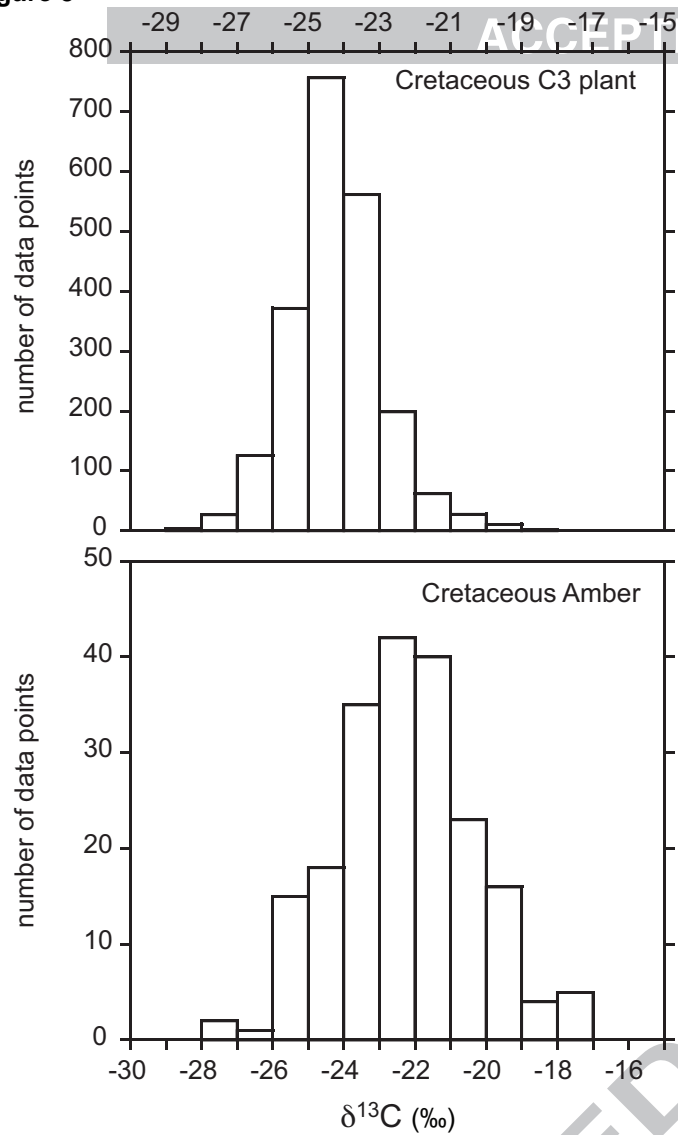
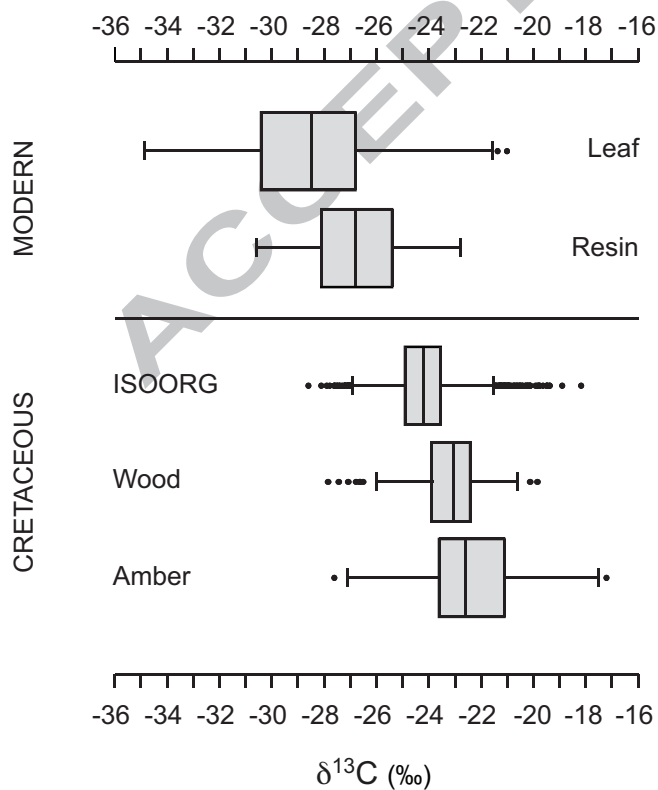
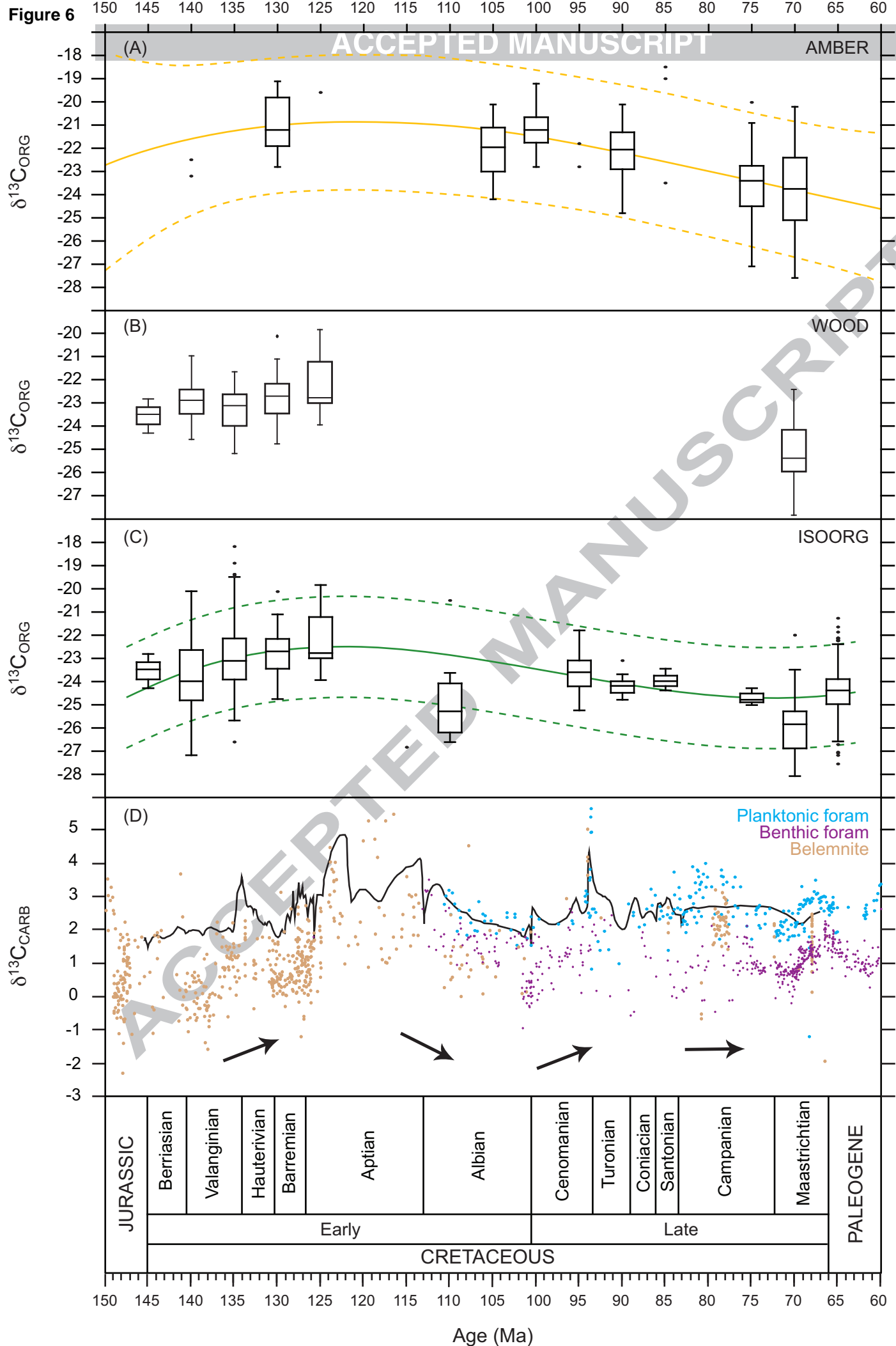
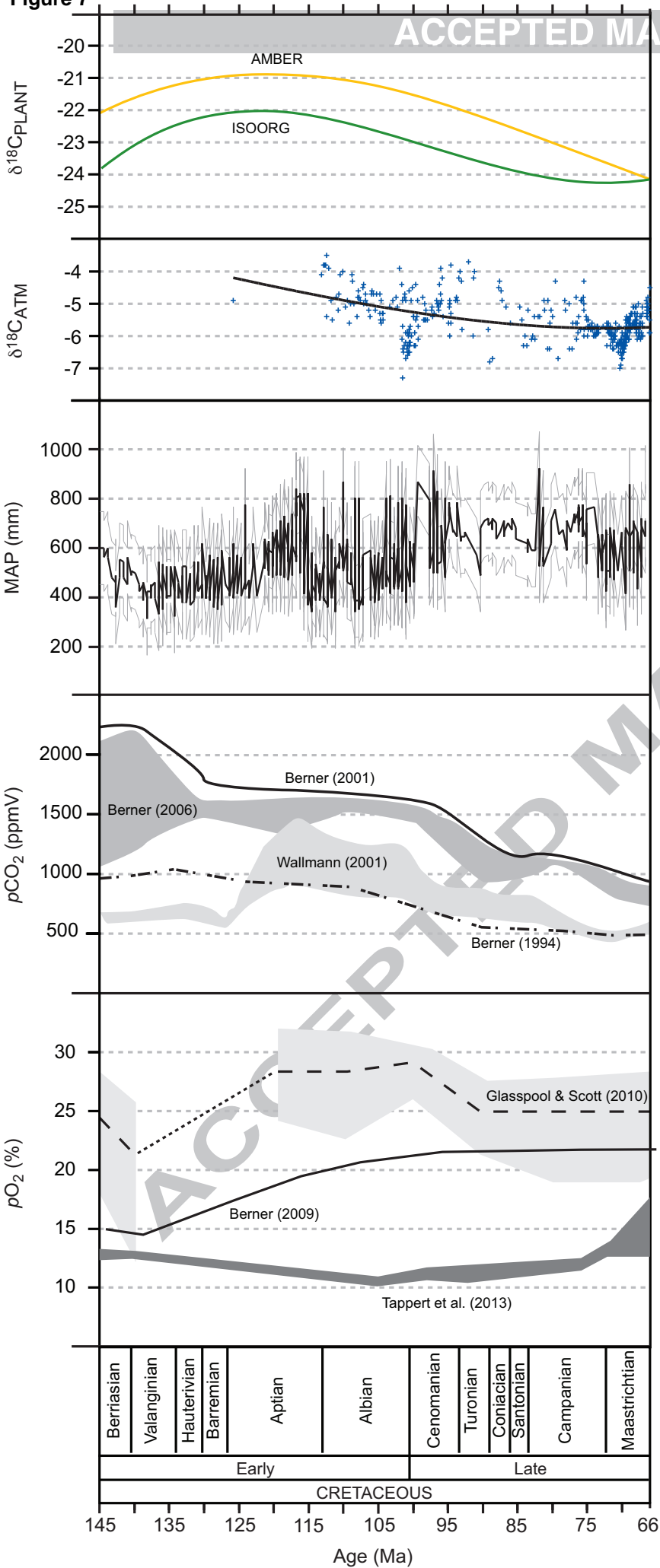
Figure 5**B**

Figure 6





1047 **Table 1.** Plant species, from which resin was collected, resin mean carbon-isotope values for
 1048 each species (mean \pm standard deviation (SD) and sample size.

1049

Species	$\delta^{13}\text{C} \pm \text{SD} (\text{‰})$	n.
<i>Abies concolor</i>	-23.7	1
<i>Abies magnifica</i>	-23.6 \pm 1.1	2
<i>Agathis lanceolata</i>	-24.5 \pm 0.2	2
<i>Agathis moorei</i>	-25.9 \pm 0.4	2
<i>Agathis ovata</i>	-25.7	1
<i>Araucaria</i> (all species listed below)	-27.1 \pm 1.4	13
<i>Araucaria columnaris</i>	-26.3 \pm 1.3	4
<i>Araucaria excelsa</i>	-28.8 \pm 0.8	4
<i>Araucaria humboldtensis</i>	-26.3 \pm 0.7	4
<i>Araucaria rulei</i>	-27.6	1
<i>Cedrus deodara</i>	-24.9 \pm 0.5	2
<i>Cupressus arizonica</i>	-29.8 \pm 0.1	2
<i>Falcatifolium taxoides</i>	-24.4	1
<i>Juniperus occidentalis</i>	-27.4	1
<i>Picea abies</i>	-27.7	1
<i>Pinus</i> (all species listed below)	-26.9 \pm 1.7	55
<i>Pinus balfouriana</i>	-24.3 \pm 0.6	2
<i>Pinus coulteri</i>	-25.8 \pm 0.32	3
<i>Pinus edulis</i>	-24 \pm 0.7	3
<i>Pinus elliotii</i>	-28.3 \pm 0.2	3
<i>Pinus jeffreyi</i>	-28.2 \pm 1.1	10
<i>Pinus lambertiana</i>	-26.5 \pm 1	5
<i>Pinus longaeva</i>	-24.6	1
<i>Pinus monophylla</i>	-24.9 \pm 0.9	5
<i>Pinus monitcola</i>	-28 \pm 2	2
<i>Pinus muricata</i>	-28.2 \pm 0.9	8
<i>Pinus ponderosa</i>	-27.2 \pm 1.3	9
<i>Pinus radiata</i>	-26.5 \pm 0.8	2
<i>Pinus sabiniana</i>	-27.2 \pm 0.7	2

1050

1051

1052 **Table 2.** Standard deviation (SD), interquartile range (IQR) and sample size (n.) of $\delta^{13}\text{C}$ data
 1053 of modern resin and leaf, and Cretaceous amber, wood and other mixed C3 plant material
 1054 (from ISOORG; TOM = bulk terrestrial organic matter). For the Cretaceous, SD and IQR
 1055 have been also calculated per each 5Myrs age bin from 65Ma to 145Ma (see text and Nordt *et*
 1056 *al.*, 2016 for explanations). Bins not listed in the table contain no data. ISOORG and wood
 1057 data are taken from Nordt *et al.* (2016) and Salazar-Jaramillo *et al.* (2016).
 1058

AGE	Type	Mean (‰)	SD (‰)	IQR (‰)	n.
Modern	Resin	-26.7	1.77	2.7	85
	Leaf	-28.4	2.52	3.6	513
Cretaceous	Amber	-22.3	1.95	2.5	201
	C3 Plant	-24.2	1.31	1.4	1384
	Charcoal	-22.9	1.55	2	192
	Coal	-24.2	1.43	1.23	95
	Leaf and cuticle	-24.7	1.72	2.14	16
	TOM	-24.4	0.98	1.1	874
	Wood	-23.1	1.31	1.47	207
AGE bin	Type		SD (‰)	IQR (‰)	n.
65Ma	C3 Plant (TOM, leaf, coal)	-24.5	0.88	1.08	677
70Ma	Amber	-23.7	1.79	2.60	40
	C3 Plant (TOM, leaf, coal)	-25.9	1.17	1.60	43
	Wood	-25.2	1.32	1.80	27
75Ma	Amber	-23.5	1.39	1.75	51
	C3 Plant (TOM)	-24.7	0.30	0.38	5
85Ma	C3 Plant (TOM)	-24	0.31	0.42	14
90Ma	Amber	-22.1	1.10	1.60	36
	C3 Plant (TOM)	-24.1	0.51	0.50	9
95Ma	C3 Plant (TOM)	-23.6	0.73	1.12	167
100Ma	Amber	-21.1	0.98	1.33	11
105Ma	Amber	-22	1.33	1.85	14
110Ma	C3 Plant (leaf)	-24.8	2.03	1.88	8
125Ma	Wood	-22.2	1.15	1.78	19
130Ma	Amber	-20.8	1.20	2.10	25
	Wood	-22.8	0.93	1.29	89
135Ma	C3 Plant (coal, charcoal)	-22.9	1.49	1.78	231
	Wood	-23.3	1.04	1.36	35
140Ma	C3 Plant (coal, wood)	-23.6	1.56	2.18	87
	Wood	-22.9	0.87	1.05	37
145Ma	Wood	-23.6	0.45	0.69	12

1059
 1060